

**Characterization of TiO₂ Photoelectrodes Fabricated via a Low Temperature
Sintering Process.**

By
Venu Gopal Patha

Submitted in Partial Fulfillment of the Requirements
for the Degree of
Master of Science
in the
Chemistry
Program

YOUNGSTOWN STATE UNIVERSITY

May, 2011

**Characterization of TiO₂ Photoelectrodes Fabricated via a Low Temperature
Sintering Process.**

Venu Gopal Patha

I hereby release this dissertation to the public. I understand that this dissertation will be made available from the OhioLINK ETD Center and the Maag Library Circulation Desk for public access. I also authorize the University or other individuals to make copies of this dissertation as needed for scholarly research.

Signature:

Venu Gopal Patha, Student Date

Approvals:

Dr. Clovis A. Linkous, Thesis Advisor Date

Dr. Timothy R. Wagner, Committee Member Date

Dr. Larry S. Curtin, Committee Member Date

Dr. Howard D. Mettee, Committee Member Date

Peter J. Kasvinsky, Dean of School of Graduate Studies and Research Date

ABSTRACT

TiO₂ photoanodes used for water-splitting solar cells or dye-sensitized solar cells (DSSC) have to meet the following properties to assure high efficiency: good connection between TiO₂ grains and a large inner surface area, TiO₂ grain shape and film conductivity. Nanocrystalline TiO₂ films are usually prepared by adding an organic binder to TiO₂ paste on glass substrates, and followed by heating at temperatures ranging from 450 to 500 °C. The organic binder is used to increase viscosity, enabling the formation of uniform TiO₂ films. Heat treatment is used to sinter the nanoparticles, as well as burn out the organic binder. In the case of composite formulations involving organic polymer electrolyte membranes, the conventional preparation technology is not suitable, because of the low temperature resistance of the polymer, on order of 150 °C. Therefore, to make thick TiO₂ films with good interconnection between the nanoparticles at low temperature, it is essential to enhance the viscosity of TiO₂ colloidal solution without using an organic binder. Possible approaches are developed by using acid-base chemistry, where the viscosity of acidic TiO₂ colloidal solution is monitored while adding ammonia solution which acts as a base. Thus the processed TiO₂ photoanode was assembled into a photoelectrochemical cell and tested by measuring *I-V* characteristics under illumination by white light from a solar simulator. TGA, DSC, IR, XRF, XRD and SEM analyses were performed to characterize the films. The low temperature process yielded titania films that were comparable to the conventional high temperature method.

ACKNOWLEDGEMENTS

I would like to thank my research advisor Dr. Clovis A. Linkous for his consistent support throughout my Masters and giving me the confidence to complete my thesis. “It wouldn’t have happened without you”. Thanks to Dr. Timothy R. Wagner, Dr. Larry S. Curtin and Dr. Howard D. Mettee for being a part of my thesis committee. I thank all the faculty and staff in the Department of Chemistry for their helping hand.

Finally would like to thank Dr. Virgil Solomon, Dr. Matthias Zeller, Raymond E. Hoff for helping us with instrumentation.

TABLE OF CONTENTS

	PAGE
TITLE PAGE.....	i
SIGNATURE PAGE.	ii
ABSTRACT.....	iii
ACKNOWLEDGEMENTS.....	iv
TABLE OF CONTENTS.....	v
LIST OF TABLES	ix
LIST OF FIGURES	ix
CHAPTERS	
CHAPTER 1	
1.1 Introduction/background:.....	1
1.2 Photovoltaic effect:	2
1.3 Semiconductors and Photoelectrochemistry:.....	3
1.4 Photoelectrochemistry in the cell when illuminated:.....	4
1.5 Dye Sensitized Solar Cells (DSSC):.....	5
1.6 DSSC working principle:.....	5
1.7 Sensitizer materials for DSSC application:.....	8
1.8 Membrane photocatalysis:	11
1.9 TiO ₂ electrode:	11
1.10 Preparation of membrane electrode assembly (MEA):.....	12
1.11 Importance of Nafion as proton exchange membrane in photoelectrochemical cells	13
1.12 Nomenclature and molecular weight:	14
1.13 Processing of semiconductor films	16
1.13.1 Coating and printing techniques:	16

1.13.2 Casting:	16
1.13.3 Spin coating:	17
1.13.4 Spray coating:	18
1.13.5 Doctor blading:	18
1.13.6 Physical evaporation:	19
1.13.7 Filament evaporation:	19
1.13.8 Electron beam evaporation:	20
1.13.9 Flash evaporation:	20
1.13.10 Sputtering:	20
1.13.11 Chemical vapor deposition:	21
CHAPTER 2	22
2.1 Research Question:	22
2.2 What is sol-gel technique and how can we use this technique for TiO ₂ films for photo electrodes	23
CHAPTER 3	
3. Materials and experimental methods:	23
3.1 Procedure for sol-gel formation:	25
Chart-I:	25
3.2 Preparation of TiO ₂ paste by using 4 different approaches	26
3.2.1 Approach I	26
3.2.1.1 Procedure for preparing sol-gel in Approach-I	27
3.2.1.2 About the reactor and operating conditions during the sol-gel preparation ..	27
3.2.2 Approach II	29
3.2.3 Approach III	29
3.2.3.1 Procedure for preparing sol-gel in Approach III	29

3.2.4 Approach IV	30
-------------------------	----

CHAPTER 4

4. Techniques used for film characterization.....	32
4.1 Thermo gravimetric Analysis (TGA)	32
4.2 Differential scanning calorimetry (DSC)	33
4.3 Attenuated Total Reflectance FT-IR spectroscopy	33
4.4 X-ray fluorescence spectroscopy.....	34
4.4.1 Basic theory and principle involved	35
4.5 Powder X-ray diffraction method.....	36
4.5.1 Theory and background	36
4.5.2 Instrumentation principle.....	38
4.6 Scanning electron microscopy (SEM).....	39
4.6.1 Working Principle.....	40
4.7 Electrochemistry and Photovoltaic measurements	41

CHAPTER 5

5. Results and discussion.....	42
5.1 Thermal decomposition of TiO ₂ sol-gel prepared from Approaches I and II	42
5.2 Thermal decomposition of TiO ₂ sol-gel prepared from Approach III.....	44
5.3 Analysis of DSC thermograms	47
5.4 Interpretation of sol-gel samples by IR spectroscopy:	48
5.5 X-ray Fluorescence spectroscopic analysis of TiO ₂ sol-gels prepared from approaches I, II & III	52
5.6 XRD analysis for particle size and shape determination.....	56
5.7 Particle size calculation by using Scherrer formula	58
5.8 Morphology of TiO ₂ films at microscopic level.....	60

5.9 Photovoltaic measurements	63
CHAPTER 6	
6.1 Conclusion:	67
6.2 Future aspects:	68
CHAPTER 7	
7. References.....	70

LIST OF TABLES

TABLE	PAGE
3.1 List of chemicals	24
3.2 Processing temperatures of different sol-gels	32
5.1 Method and experimental parameters for sol-gel prepared from Approach I and II	44
5.2 Method and experimental parameters for sol-gel prepared from Approach III.	45
5.3 Unit cell parameters of TiO ₂	58
5.4 Details of photoelectrochemical cell	65
5.5 Photo voltages of TiO ₂ photoelectrodes prepared from Approaches I, II and III	67

LIST OF FIGURES

FIGURE	PAGE
1.1 Electrochemical cell with light illuminating a semiconductor electrode	5
1.2 Schematic representation of Gratzel cell working principle	8
1.3 Ruthenium compound sensitizers and the TiO ₂ film samples With dye adhesion	9
1.4 Incident photon to current conversion efficiency as a function of the wavelength for the standard ruthenium sensitizers N3 (red line), the black dye N749 (black curve), and the blank nanocrystalline TiO ₂ film (blue curve)	9
1.5 Molecular structure of Nafion	14

3.1 Model 4544 High Pressure Reactor, 600 mL, Moveable Style Vessel, With heater lowered, and a 4848 Controller shown with optional Expansion Modules.....	28
3.2 Doctor blade TiO ₂ paste on ITO glass substrate with squeegee	30
4.1 Core electronic transitions in an atom	36
4.2 Powder X-ray diffraction instrumentation	38
5.1 TGA thermogram of anhydrous ammonium acetate	42
5.2 TGA thermogram of unsintered TiO ₂ gel prepared from Approach I	43
5.3 TGA thermogram of unsintered TiO ₂ gel prepared from Approach II.....	43
5.4 TGA thermogram of unsintered TiO ₂ gel prepared from Approach III.....	45
5.5 Overlay of TGA thermograms of unsintered TiO ₂ gels prepared from Approaches I, II and III.....	46
5.6 Transitions occurring in DSC curve of TiO ₂ gel prepared from approach I.....	48
5.7 IR spectrum of ammonium acetate	49
5.8 IR spectrum of unsintered TiO ₂ gel prepared from Approach I	49
5.9 IR spectrum of sintered TiO ₂ gel prepared from Approach-I.....	50
5.10 IR spectrum of unsintered TiO ₂ gel prepared from Approach-II.....	50
5.11 IR spectrum of sintered TiO ₂ gel prepared from Approach-II.....	50
5.12 IR spectrum of unsintered TiO ₂ gel prepared from Approach-III	51

5.13 XRF spectra showing elements in TiO ₂ sol-gel sample prepared	
From Approach I.....	53
5.14 XRF spectra showing elements in TiO ₂ sol-gel sample prepared	
From Approach II	54
5.15 XRF spectra showing elements in TiO ₂ sol-gel sample prepared	
From Approach III	55
5.16 Overlay of XRF spectra showing the elements in TiO ₂ sol-gel samples	
Prepared from Approaches I, II and III.....	56
5.17 XRD pattern of TiO ₂ sol-gel sample prepared from Approach I;	
Blue lines correspond to anatase phase TiO ₂ , while red lines	
Correspond to SnO ₂	57
5.18 XRD pattern of TiO ₂ sol-gel sample prepared from Approach II;	
Blue lines correspond to anatase phase TiO ₂ , while red lines	
Correspond to SnO ₂	59
5.19 XRD pattern of TiO ₂ sol-gel sample prepared from Approach III;	
Blue lines correspond to anatase phase TiO ₂ , while red lines	
Correspond to SnO ₂	60
5.20 Images of TiO ₂ sol-gel films prepared from Approach I, which are coated	
On ITO glass substrates	61

5.21 Images of TiO ₂ sol-gel films prepared from Approach II, which are coated	
On ITO glass substrates	62
5.22 Images of TiO ₂ sol-gel films prepared from Approach III, which are coated	
On ITO glass substrates	63
5.23 Photovoltaic measurements of TiO ₂ Photoanodes made by connecting	
And placing the cell with potentiostat and solar simulator	64
5.24 Voltammograms of TiO ₂ photo anode in dark and light conditions prepared	
From sol-gel Approach I.....	65
5.25 Voltammograms of TiO ₂ photo anode in dark and light conditions prepared	
From sol-gel Approach II.....	66
5.26 Voltammograms of TiO ₂ photo anode in dark and light conditions prepared	
From sol-gel Approach III	69

Chapter 1

1.1 Introduction/background:

World energy consumption is increasing ever faster, according to the EIA (U.S energy information administration). Nearly 500 quads of energy are being used per year worldwide. Almost ninety percent of the energy used in the world is being supplied from fossil fuels yet it has been estimated that the economically accessible fossil fuel resources will be depleted soon, according to “Hubbard’s” peak theory. The theory tells that as the world’s energy demand increases, the production rates of fossil fuels are also increased. The relationship continues up to a time when there will be no economical fossil fuel reserves available and thus, after this time, the production of primary fuels starts to decrease and according to supply/demand relationship, the fuel prices start to increase also the production peaks out. To meet the daily requirements, new technologies for the generation of new types of energy must be developed. Hydrogen is an efficient energy carrier with high energy density (33,900 cal/g) and is also environmentally friendly. Currently, more than 95% of hydrogen is produced by catalytic thermochemical conversion processes, which involve energy losses and the release of greenhouse gases.[1] With the evolution of cyanobacteria over three billion years ago, nature has already presented a way to split water into hydrogen and oxygen using sunlight. Several studies have focused on emulating the natural process of photosynthesis, in search of new ways to exploit hydrogen as an energy source. The utilization of metal oxides for light harvesting and photoelectrochemical (PEC) water splitting is a promising avenue for sustainable hydrogen production. In 1972, Fujishima and Honda first used n-type semiconductors like TiO_2 photoanodes for hydrogen evolution. Metal oxides such as

TiO₂, ZnO, WO₃, and Fe₂O₃ have subsequently been studied by many research groups for developing PEC cell devices [2]. For hydrogen generation in PEC cells, a minimum of 1.23 V must be generated between the anode and cathode. Apart from this, the efficiency and stability of photoelectrodes are also key factors. TiO₂ is especially attractive as a photoelectrode because of its high efficiency, chemical and optical stability, and environmental and biological compatibility.

1.2 Photovoltaic effect:

The photovoltaic effect and photoelectric effect are two different processes and should be distinguished. The photovoltaic effect is the creation of voltage in a material upon exposure to light. Even though the photovoltaic effect is related to the photoelectric effect, in the photoelectric effect electrons are ejected from a material's surface upon exposure to radiation of sufficient energy. In the photovoltaic effect, the generated electron is transferred between different energy bands within the material, which build up the voltage between two electrodes.

1.3 Semiconductors and Photoelectrochemistry:

Generally all atoms are made up of orbitals, which are filled or left empty by electrons. When these orbitals are brought together they form new molecular orbitals, which have different energies. In conductors the valence band (filled bonding orbitals) and conduction band (empty anti bonding orbitals) are overlapping, so very little energy is required to promote an electron to empty anti bonding orbital. If the conduction and valence bands are not overlapping then the band gap is very high and these materials are called as insulators. However if the band gap is small, electrons can be transferred to the conduction band thermally, leaving a hole in the valence band. These materials are called

semiconductors. A semiconductor may be either p-type or n-type. In a p-type semiconductor, an impurity has been added which has empty orbitals just above the valence band in the original material, so that the electrons can be promoted from the valence band to these empty energy levels leaving holes in the band. In n-type semiconductors, an impurity is added which has a filled energy level that is just below the empty conduction band. Electrons are donated to the conduction band; thus the majority of charge carriers are negative. Titanium dioxide is one of the promising candidates for photo electrodes used for solar-hydrogen.

Like other metals TiO_2 also exhibits outstanding resistance to corrosion and photocorrosion in aqueous environment. Apart from this; TiO_2 has many more functional properties:

- TiO_2 is reactive with both light and water
- Properties of TiO_2 can be easily altered by varying the defect chemistry and the related electronic structure through alteration of the oxygen nanochemistry
- TiO_2 is less expensive than other photosensitive materials, so it can replace silicon in photovoltaics.
- TiO_2 is environmentally friendly and its reserves are abundant.

With all these functional properties, TiO_2 has achieved vast importance in many applications:

- Photoelectrochemical generation of hydrogen (solar-hydrogen) [3]
- Decontamination of water from bacteria, viruses and organic compounds.
- Self-cleaning building materials.

- Paving materials leading to reduction of air pollution.
- Antiseptic paints and coatings.
- Chemical gas sensors.
- Skin and stomach anticancer treatments.
- Antifogging mirror and glass coatings.
- Generation of PV electricity.
- Purification of air

1.4 Photoelectrochemistry in the cell when illuminated:

Fujishima and Honda first showed that illumination of n-type semiconductors greatly reduced the voltage required to decompose water. Generally to split water, a potential difference of 1.23V must be established between the anode and cathode. In a typical electrochemical cell the anode and cathode are n-type semiconductor and platinum wire, respectively. The semiconductor electrode is irradiated to promote an electron from valence band to conduction band, which results in generation of current through the external circuit. Thus the hole left in the valence band results in oxidation of water at the semiconductor, and the electron obtained in the conduction band will cause reduction of hydrogen ions at a platinum counter electrode. [4] The schematic of the process explained can be seen in the Figure1.1 below:

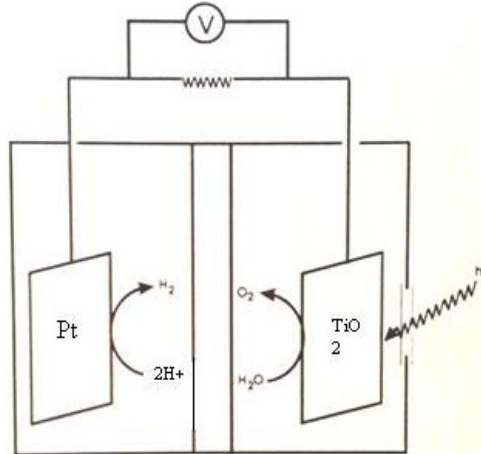


Figure 1.1: Electrochemical cell with light illuminating a semiconductor electrode [4]

1.5 Dye Sensitized Solar Cells (DSSC):

Dye sensitized solar cell (DSSC) is one energy source in the photoelectrochemical cell family. DSSC is a solar cell using wide band gap semiconductor and sensitizer loading to adsorb light, then, converting the light energy into electricity. Comparing to the silicon based solar cell, DSSC manufacturing process is easier and less expensive. Wide band gap semiconductor is also able to provide water-splitting energy for further solar fuel because it is more stable in liquid comparing to the silicon semiconductors and higher output voltage. The dye sensitize theory was first applied for solar cell in 1970's, but the efficiency was only 0.1% [5]. In 1991, Michael Gratzel described a DSSC with nano-crystalline TiO_2 , for the anode material, and a ruthenium complex sensitizer with high turnover number, achieving 7% efficiency [6]. Gratzel established a basic DSSC structure, which most DSSC investigators adapted or modified.

1.6 DSSC working principle:

In dye-sensitized solar cell (DSSC), light is captured by a dye first and then passes through the nano-crystalline anode material to a conductive glass substrate, such as tin-

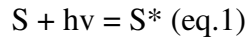
doped indium oxide (ITO) or fluorine-doped tin oxide (FTO) glasses. According to the equation $E=hc/\lambda$ (where E stands for the energy of light, h stands for the Planck's constant, c stands for the speed of light and λ stands for the wavelength of light), anatase TiO_2 can absorb ultra-violet light which has wavelength less than 387 nm because it has a band gap of 3.2 eV, but it cannot absorb visible light which is between 400 nm and 700 nm. In order to increase the efficiency, dye is needed to capture visible light. Dye will be excited by sunlight and charges can then be transferred from the metal center of the dye, such as ruthenium, to TiO_2 by ligand attached on the TiO_2 . The excited energy level of the dye is higher than the TiO_2 anode conduction band and the electrons will inject into the semiconductor with femto-seconds speed, which is a very fast rate [7].

The back electron transfer speed is much lower and the electrolyte to oxide dye charge transfer is also very fast in order to regenerate the oxide dye. That is the principle that the device is able to collect electrons in nano-semiconductor powder. An ideal dye should have larger excited energy level comparing to the TiO_2 , wide absorption range for visible light and high turnover number [7]. Ruthenium complex is the most widely used dye [6]. After electrons inject into the nano-crystalline TiO_2 , electrons will move by diffusion to the conductive glass and reach the outer circuit to the cathode, which is usually made by platinum. Finally the reduction and oxidation of electrolyte, which already supply electrons to the oxide dyes, are completed, and the circuit can be showed in Figure 1.2. Typical electrolyte is I^-/I_3^- because it provides fast dye regeneration speed and it is chemically stable. The most common cathode material is platinum, which has good conductivity and also reflects incident light to dye- TiO_2 layer, and this enhances the efficiency. In Figure 1.2, the TiO_2 Fermi level and the oxide electrolyte energy level will

determine the maximum voltage.

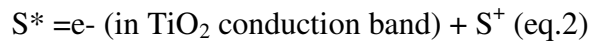
The chemical reactions of this DSSC can be given as follows:

(1) Dye is excited by light and the electrons jump to the excited state from the ground state.

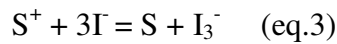


S: ground state of dye S*: excited state of dye S⁺: Oxidized state of dye

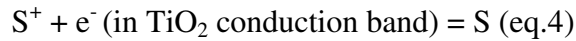
(2) Electrons inject into the conduction band of semiconductor from the dye-excited state.



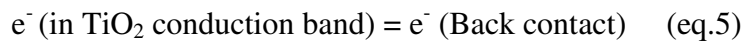
(3) Electrolyte redox couple reaction is.



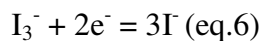
(4) Recombination between electrons in TiO₂ conduction band and oxidized dye occurs



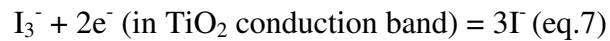
(5) Electrons in conduction band conduct to outer circuit



(6) Electrons in nano-crystalline semiconductor combine with I₃⁻ ions



(7) I₃⁻ ions spread to the counter electrode and electrons lead to the re-generation of I⁻ ions



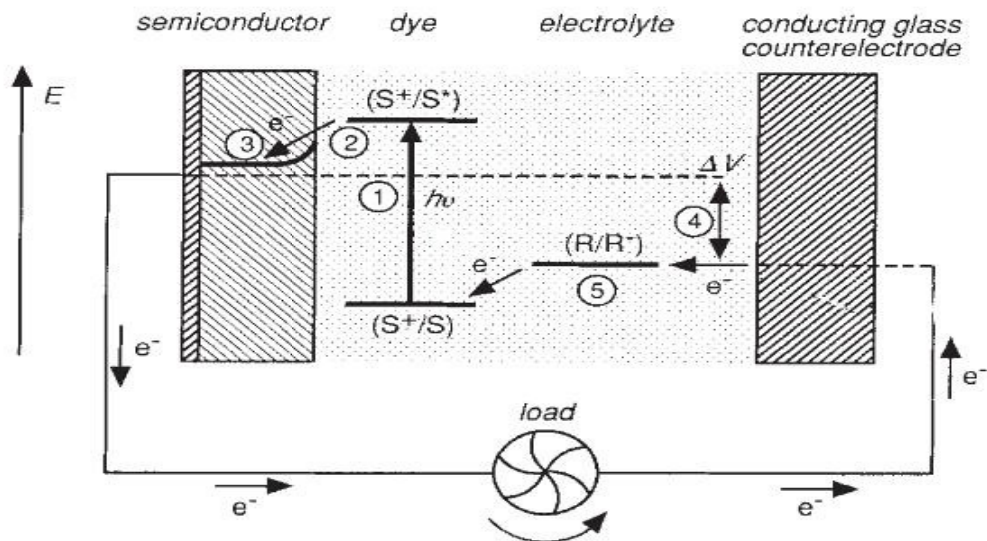


Figure 1.2: Schematic representation of Gratzel cell working principle. The numbers in this figure indicate the reactions take place in sequence [6].

1.7 Sensitizer materials for DSSC application:

The theoretical requirements of DSSC sensitizer are: higher energy level of the excited dye comparing to the TiO_2 or other anode semiconductor conduction band edge, slow back electron transfer, but fast dye to TiO_2 transfer. The electron transfer from electrolyte to oxide dye must be fast enough to regenerate it to complete the overall electron transfer loop. The turnover number must be high for long-term usage. The sensitizers with highest efficiency are ruthenium complex today. Commercial available ruthenium based dye such as cis-Di-(thiocyanato) bis (2, 2 ϕ bipyridyl)-4, 4 ϕ -dicarboxylate) ruthenium-(II), coded as N3 or N-719 dye depending on whether it contains four or two protons [8,9], have been found to be outstanding solar light absorbers and charge-transfer sensitizers. The performance of this red ruthenium complex is unmatched for a long time by any other dyestuff. However, a black dye has been discovered that shows a performance comparable to that of N3 as a charge-transfer sensitizer in the DSSC a few years ago [10]. The structure of these sensitizers is shown in Figure 1.3. Manipulating the ligands

can change the adsorption spectrum. It is one of the most powerful parts of sensitizer investigation. Figure 1.4 shows the adsorption spectrum of TiO₂ and these commercial available dyes.

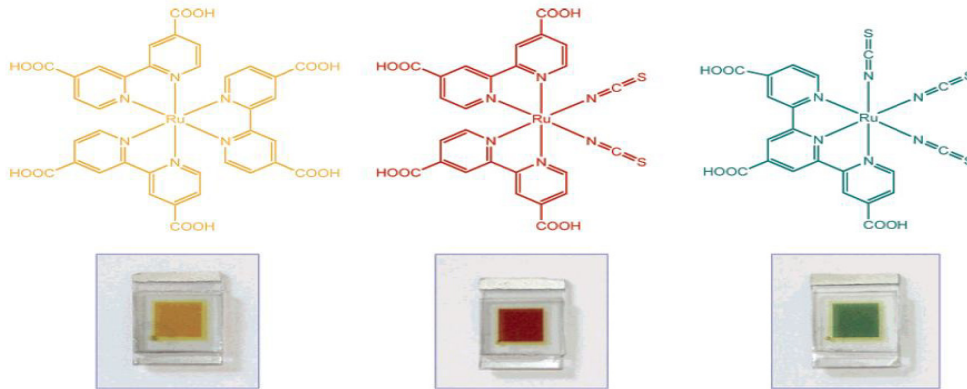


Figure 1.3: Ruthenium compound sensitizers and the TiO₂ film samples with dye adhesion [9].

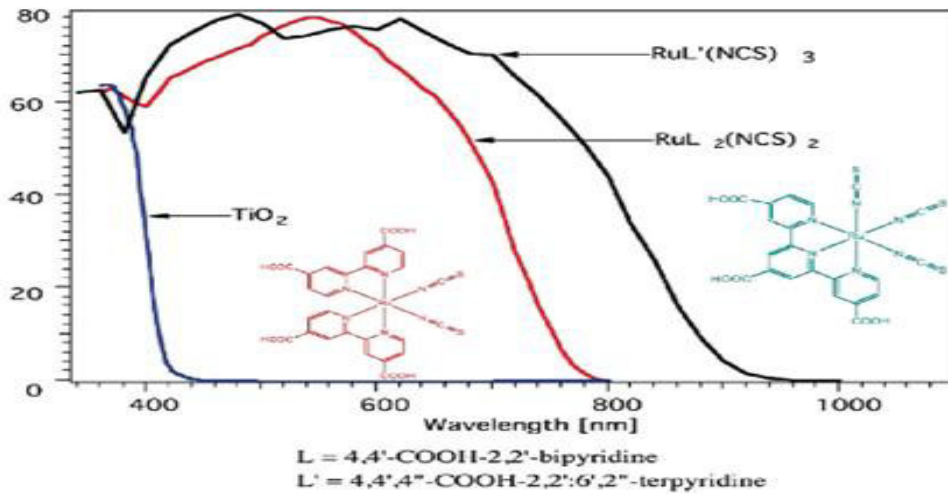


Figure 1.4: Incident photon to current conversion efficiency as a function of the wavelength for the standard ruthenium sensitizers N3 (red line), the black dye N749 (black curve), and the blank nanocrystalline TiO₂ film (blue curve) [11].

There is a summary made by Gratzel [7] about the description of charge behaviors between sensitizer and TiO₂:

- Electron injection into TiO₂: following the light absorption of the Ru complex, the

electron injection into the conduction band is in the sub-ps to ps range.

- Back electron transfer: the rate constant for the back electron transfer (dark reduction in the absence of externally added electron donors) however is much smaller for several reasons, typically several μs .
- Reduction of triiodide by e_{cb}^- : another important recombination process is reduction of I^3^- in the electrolyte by conduction band electrons. The exchange current density, j_0 of the reverse saturation current of this process has been measured in the range 10 to $11 \times 10^{-9} \text{ A cm}^{-2}$, depending on the electrolyte. Surface treatment of the electrode can alter these values drastically.
- The electron movement (percolation) in the nanocrystalline TiO_2 electrode to the back contact is significantly slower than in single crystal TiO_2 . Studies have shown that the photocurrent transients, following UV excitation of TiO_2 particles from an ns pulsed laser, decay in the ms to s range.
- The exchange current density for the reduction of triiodide at the counter electrode ITO coated with a catalytic amount of Pt, has been measured to be 0.01 to $2 \times 10^{-1} \text{ A cm}^{-2}$.
- Reduction of the oxidized dye by iodide occurs on a timescale of 10^{-8} s .

The metal to ligand charge transfer is important because it will determine the injection speed and backward electron transfer rate. As mentioned before, the charges can be separate due to the huge speed difference [7]. Usually carboxylate group is applied to attach the ruthenium dye on the TiO_2 surface, like N3, N719 and black dye. The ruthenium center will be excited after lighting and inject the electrons through the metal

to ligand charge transfer. The reason that the backward charge transfer is much slower because the back reaction of the electrons with the oxidized ruthenium complex involves a d orbital localized on the ruthenium metal. Its electronic overlap with the TiO₂ conduction band is small and is further reduced by the spatial contraction of the wave function upon oxidation of Ru (II) to Ru (III). Thus, the electronic coupling element for the back reaction is 1-2 orders of magnitude smaller for the back electron transfer as compared to injection reducing the back reaction rate by the same factor.

1.8 Membrane photocatalysis:

The working principle of Photo Electro Chemical Membranes PEM, reactions on each electrode and thermodynamics of the cell need to be known to better understand the PEM electrolyzers. Briefly water electrolysis is a chemical reaction where water is the reactant and hydrogen and oxygen are the products. The electrolysis cell is a reaction medium composed of a membrane electrode assembly (MEA), the electric current collectors, gas distribution layers and the gaskets.

1.9 TiO₂ electrode:

The nano-crystalline semiconductor anode is not only where the sensitizers adhere, but also where the charge transfer occurs. Consequently, it is acknowledgeable that the quality of the semiconductor electrode directly affects the efficiency of DSSC. Reducing charge recombination is the most direct means to improve DSSC efficiency, and the quality of TiO₂ film is one of the most important keys. There are four fundamental requirements of the electrode material: large surface area and roughness, sponge-like nano-crystalline structure with good electronic contact. The anode material structure should allow electrolyte redox couple regenerates the oxide dye and charge should also

be able to rapidly inject into the semiconductor. At the meantime, backward charge recombination should be the slowest step. TiO_2 is an ideal material with appropriate band gap and electronic properties as mentioned. It has additional advantages like non-toxic, stable in water and better anti-corrosion property comparing to narrow band gap semiconductor material like silicon. TiO_2 has three kinds of crystal structure: anatase, rutile and brookite. Brookite only exists in natural ores and it cannot be synthesized in industry. Anatase has a band gap of 3 eV and rutile has a band gap of 3.2 eV. The conduction band density of anatase in Ti 3d is higher than that of rutile, which makes it easier to accept electrons from the top of valence band (O 2p). That is the reason that anatase TiO_2 has better performance comparing to rutile [12, 13, 14]. These mechanics will determine the efficiency of the DSSC. TiO_2 electrode is one of the most important keys to increase the efficiency because it is where sensitizers load and the electrons transfer happen. The requirements of the TiO_2 film is related to these mentioned concepts. The purpose of this study is to manufacture a thick film from TiO_2 paste, which is appropriate for mass production and able to lower the DSSC or the photoelectrochemical cell cost.

1.10 Preparation of membrane electrode assembly (MEA):

Generally all MEA's are prepared by coating anode and cathode materials on either side of a Nafion membrane (which is an efficient proton conductor because of sulfonation). Typical MEA's have the gas-diffusing layer for both anode and cathode, which are created by using an optimized procedure [15]. Firstly the nafion membranes were preconditioned in 5% hydrogen peroxide and then in altering baths of boiling 1M

H₂SO₄. Then a carbon paper is used to anchor the TiO₂ photocatalyst particles on one side and Pt particles on cathode on other side of membrane.

Deionized water is generally used for PEM electrolysis in order to prevent impurities from poisoning the catalyst on each side of the membrane. Water, when passed into the electrolyzer, is split into oxygen, two protons and two electrons at the anode, by applying DC voltage at standard temperature and pressure. Then the protons pass through the proton exchange membrane and at the cathode they combine with electrons coming from the external power source to form hydrogen gas.

1.11 Importance of Nafion as proton exchange membrane in photoelectrochemical cells:

The Proton exchange membrane is a proton-conducting polymeric membrane, which acts as an electrolyte for both the fuel cell (Fuel cell is a electrochemical that converts chemical from a fuel to electric energy) and the electrolysis application. General Electric developed the first PEM used in fuel cells in early sixties for use in a space mission for NASA. This premature copolymer showed insufficient oxidative stability under its operating conditions and could work properly for only 500 h during the mission. A major breakthrough in PEM technology came up by introducing perfluorosulfonic acid membranes called Nafion perforated membranes in 1960s by Walther Grot of Dupont.

Nafion's unique ionic properties are a result of incorporating perfluorovinyl ether groups terminated with sulfonate groups onto a tetrafluoroethylene (Teflon) backbone. Nafion has received a considerable amount of attention as a proton conductor for proton exchange membrane (PEM) fuels cells because of its excellent thermal and mechanical staility.

1.12 Nomenclature and molecular weight:

Nafion can be produced as both a powder resin and a copolymer. It has various chemical configurations and thus several chemical names in the IUPAC system. The molecular weight of Nafion is uncertain due to differences in processing and solution morphology. The structure of a Nafion unit, shown in the Figure 1.5 below illustrates the variability of the material. For example, the most basic monomer contains chain variation between the ether groups (the z subscript). Conventional methods of determining molecular weight such as light scattering and gel permeation chromatography are not applicable because Nafion is of course insoluble, although the molecular weight has been estimated at 10^5 - 10^6 Da. Instead, the equivalent weight (EW) and material thickness are used to describe most commercially available membranes. The EW is defined as the weight of Nafion (in grams) per mole of sulfonic acid group. For example, Nafion 117 represents 1100 g EW + 0.007 inch in thickness. In contrast to equivalent weight, conventional ion exchange resins are usually described in terms of their ion exchange capacity (IEC), which is inversely proportional to the equivalent weight.

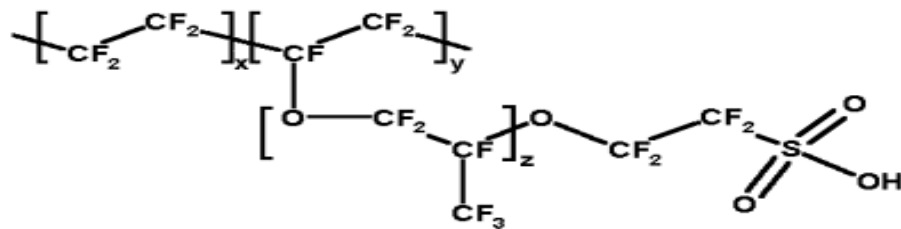


Figure 1.5: Molecular structure of Nafion

Typically perfluorosulfonic acid membranes are poor proton conductors unless water is present in the medium. Therefore the hydration of PEM is very important with respect to the performance of the cell. Although this is important for fuel cells, it is

usually not the case for the electrolysis application since one of the sides of the membrane is always exposed to water as reactant.

Many research groups reported that a typical proton exchange membrane had to match the following requirements in order to be used in fuel cells and eletrolyzers:

- The membrane must have good thermal, oxidative and hydrolytic stability (Nafion is stable up to 200 °C).
- Good film formation and high proton conductivity (even at low humidity)
- The membrane should have low electronic conductivity and good water retention properties.
- The membrane should be capable of fabrication into MEA's

Perfluorosulfonic acid polymers have been considered as unique and nearly optimal materials to serve as separators in both eletrolyzers and PEM fuel cells. However, they cannot meet the most important requirement: the cost of a PEM is nearly about (700-800 \$/m²).

If we clearly observe the molecular structure of Nafion, the hydrophilic regions around the clusters of sulphonated side chains enable water uptake. The water absorption process can increase the weight of the membrane as much as 30%. Hydrogen ions are weakly attracted to the SO₃⁻ group and so are able to move in these hydrated regions of the membrane. Though the hydrated regions are separate from each other, hydrogen ions are able to move through the supporting structure. This situation decreases the proton conductivity, however in a well-hydrated membrane, 20 water molecules could exist for

each SO_3^- side chain [16]. The thickness of the membrane is a crucial parameter. If the thickness is increased, the hydration of the membrane is generally decreased, which results in relative poor ion conductivity. But as the thickness is increased, gases such as hydrogen, crossover decreased. Since the hydration of the membrane is usually not a problem in the electrolysis application, thicker membranes are preferred for these devices.

1.13 Processing of semiconductor films:

Semiconductor film formation is an important step in developing a photoelectrochemical cell for water splitting. Various methods are available for processing semiconductors. A brief explanation about these techniques is as follows:

1.13.1 Coating and printing techniques:

Coating and printing are two different techniques and it is important to distinguish them, at least in this context. Generally printing is used to describe a method by which a layer of ink is transferred from a stamp to a substrate by a reversing action. A good example is an office stamp, which does the exact job. Coating is used to describe a process by which a layer of ink is transferred to the substrate by essentially pouring, painting, spraying, casting or smearing it over the surface. Printing techniques include screen-printing, pad printing, gravure printing, flexographic printing and offset printing. Coating techniques include spin coating, doctor blading, casting, painting, spray coating, slot-die coating, curtain coating, slide coating and knife-over-edge coating [17].

1.13.2 Casting:

This is probably the simplest film-forming technique available. The advantage is that no equipment is needed apart from a very horizontal work surface. The procedure is

to simply cast a solution onto a substrate followed by drying. While it is possible to prepare films of good quality and also thick films, the technique suffers from a lack of control over the film thickness and often picture framing effects are observed near the edges of the film or precipitation during drying. In cases where the surface tension of the liquid dominates the drying is inhomogeneous. Also there is a requirement that the material to be coated has a high solubility in the solvent used if crystallization or precipitation is to be avoided.

1.13.3 Spin coating:

The typical spin coating operation involves application of a liquid to a substrate followed by acceleration of the substrate to a chosen rotational speed. Alternatively the liquid solution may be applied while the substrate is spinning. The angular velocity of the substrate with the overlying solution results in the ejection of most of the applied liquid where only a thin film is left on the substrate. The thickness, morphology and surface topography of the final film obtained from a particular material in a given solvent at a given concentration is highly reproducible.

Other film techniques such as slide coating and curtain coatings are somewhat relevant techniques, as these techniques allow simultaneous coating of multilayer films (up to 18 layers). The only challenge with these coating techniques is that a very rapid ink flow is required. This implies that a large web speed is needed for the coating to work properly when thin films are prepared.

1.13.4 Spray coating:

This technique mainly forces the printing ink through a nozzle where by a fine aerosol is formed. A carrier gas and electrostatic charging may be involved to aid in directing the aerosol at the surface that is to be coated.

1.13.5 Doctor blading:

This technique is a focus in our research because of its compatibility and feasibility. Doctor blading technique is a good technique for the formation of films with well-defined thickness. In contrast to spin coating, the technique consumes the coating solution quite effectively, and with some practice the loss of coating solution can be minimized to less than 5%. The technique works by placing a sharp blade at a fixed distance from the substrate surface that is to be coated (typically 10-500 μm). The coating solution is then placed in front of the blade that is then moved linearly across the substrate leaving a thin wet film after the blade. The final wet thickness of the film is ideally half the gap width but may vary due to the surface energy of the substrate, the surface tension of the coating solution and the viscosity of the coating solution. It also depends on the meniscus formed between the blade and the wet film on the trailing edge of the blade, which is related to the shear field (proportional to the speed of the blade). The final dry thickness of the coated film, d , can be calculated from the empirical relationship

$$d = 1/2(g*c/\rho),$$

Where g is the gap distance between the blade and the substrate in, c is the concentration of the solid material in the ink in g cm^{-3} and, ρ is the density of the material in the final film in g cm^{-3} .

Apart from these techniques for film deposition, there are some other techniques like physical and chemical vapor deposition, epitaxial growth, and sputtering [18], which include vacuum chambers operated at different pressure levels. Brief descriptions of these techniques are as follows:

1.13.6 Physical evaporation:

Physical evaporation is the oldest method for depositing metal films. Aluminum and gold are heated to the point of vaporization, and then evaporate to form a thin film covering the surface of the target support. To improve the efficiency of material transfer, evaporation is performed under vacuum conditions.

A basic vacuum deposition system consists of a vacuum chamber, a mechanical roughing pump, a diffusion pump or turbomolecular pump, valves, vacuum gauges, and other instrumentation. In operation process, the roughing valve is opened first, and the mechanical pump lowers the vacuum chamber pressure to an intermediate vacuum level of approximately 1 pascal (Pa). If a higher vacuum level is needed, the roughing valve is closed, and the foreline and high-vacuum valves are opened. The roughing pump now maintains a vacuum on the output of the diffusion pump. A liquid-nitrogen cold trap is used with the diffusion pump to reduce the pressure in the vacuum chamber to approximately 10^{-4} Pa. Ion and thermocouple gauges are used to monitor the pressure at a number of points in the vacuum system, and several other valves are used as vents to return the system to atmospheric pressure.

1.13.7 Filament evaporation:

In this technique the vacuum system mainly consists of a filament, which is heated to high temperature, small metal loops are hung from a filament, which is formed by a

refractory metal such as tungsten. Evaporation is accomplished by gradually increasing the temperature of the filament until the metal loops melt and wet the filament. The substrate, which is to be coated, is mounted near the filament and thus covered by thin film of evaporating metal.

1.13.8 Electron beam evaporation:

In an electron beam evaporation system, the high temperature filament is replaced with an electron beam, which has energy up to 15 KeV. When these high intensity electron beams focused on the target surface, the energy from the electron beam makes the surface to melt. Thus the material evaporates from the source and covers a substrate, with a thin layer of film. The substrates mounted above the source are typically rotated around the source during deposition to ensure uniform coverage.

1.13.9 Flash evaporation:

Flash evaporation uses a fine wire as the source material, and a high- temperature ceramic bar is used to evaporate the wire. The wire is fed continuously and evaporates on contact with the ceramic bar. Flash evaporation can produce relatively thick films, as in an electron beam system, without any problems associated with radiation damage.

1.13.10 Sputtering:

Sputtering is achieved by bombarding a target with energetic ions, typically Ar^+ . When the atoms at the target surface are hit by these ions, they become loose and are transported to the substrate, where deposition occurs. Electrically conductive materials such as Al, W, and Ti can use a dc power source, in which the target acts as the cathode in a diode system.

In sputter deposition, there is a threshold energy that must be exceeded before sputtering occurs. The sputtering yield represents the number of atoms liberated from the target by each incident atom, and it increases rapidly with energy of the incident ions. Systems are usually operated with energy large enough to ensure a sputtering yield of at least unity. Sputtering can be used to deposit a broad range of materials. In addition, alloys may be deposited in which the deposited film has the same composition as the target. An example is the Al-Cu-Si alloy commonly used for metallization in integrated circuits.

1.13.11 Chemical vapor deposition:

Chemical vapor deposition (CVD) forms thin films on the surface of a substrate by thermal decomposition or reaction of gaseous compounds. The desired material is deposited directly from the gas phase onto the surface of the substrate. CVD can be performed at pressures for which the mean free path for gas molecules is quite small, and the use of relatively high temperature can result in excellent conformal step coverage over a broad range of topological profiles.

All these techniques are used to process different kinds of semiconductor films on different substrates. In our research we are using doctor blading because of its compliance and improved efficiency of the processed film by doctor blading. Also it avoids the use of vacuum chamber [19].

Chapter 2

Research Problem and Approaches

2.1 Research Question:

Our main purpose of research is to develop low cost and highly efficient TiO₂ films prepared at low temperature and can be coated on perforated nafion membranes, which serve as photo electrodes in flexible photoelectrochemical cell through which hydrogen is produced by photoelectrolytic water splitting. In order to achieve this goal we developed four different types of TiO₂ films using 4 different recipes based on sol-gel technique at different temperatures.

2.2 What is sol-gel technique and how can we use this technique for developing TiO₂ films for photoelectrodes?

Sol can be defined as a colloidal suspension of very tiny solid particles in a continuous liquid medium; these sols are quite stable and show Tyndall effect. Sols are the precursor molecules for integrated networks called gels. Generally these sols are metal alkoxides and metal chlorides, which undergo various forms of hydrolysis and polycondensation reactions.

Sol-gel technique is also called a chemical solution deposition method, which is a wet chemical technique. This technique is mainly used in materials and ceramic engineering disciplines for fabrication of materials. Generally sol-gels are versatile materials which are made by condensing a solution of metal oxide precursors into a three dimensional network. These gels are biphasic systems in which a continuous fluid phase fills the space inside a polymerized network. The gels can be dried in a controlled fashion

to produce porous solid films with unique thermal, mechanical, optical and chemical properties.

Chapter 3

3. Materials and experimental methods:

Our research objective is to prepare a suitable photoelectrode, which can be assembled in a photoelectrochemical cell for hydrogen production by water splitting. In order to produce this photoelectrode a suitable photo catalyst must be prepared, which should fulfill basic requirements such as film conductivity, mechanical strength in contact with electrolyte, good connections between particles, (without using any organic binder) and large surface area. Thus the films were fabricated with TiO₂ paste by using a doctor blade coating technique. The chemicals used in this entire work are listed in the following Table 3.1:

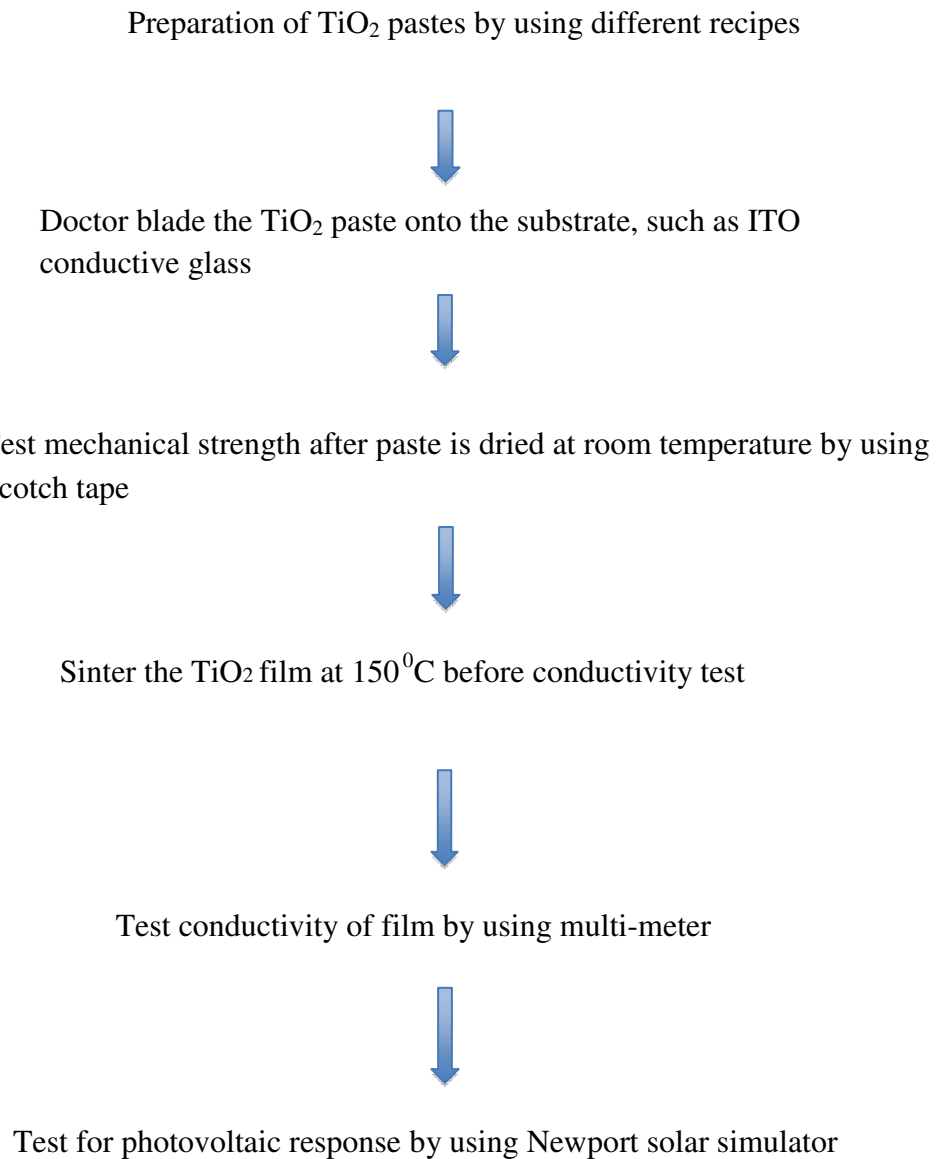
Table 3.1: List of chemicals

Chemicals	Manufacturer	Purity	Purpose of usage
P25Titanium Dioxide	Degussa, Japan		TiO ₂ particles
Titanium(IV) isopropoxide (TTIP)	Aldrich	99.99%	TiO ₂ particles
Isopropyl alcohol	Pharmaco-AAPER	99%	Alcohol
Acetic acid, glacial	Pharmaco-AAPER	99.7%	Acid
Ammonium hydroxide	Pharmaco-AAPER	28-30%	Base
Di-ethanol amine (DEA)	Fisher scientific		Binder
Sodium hydroxide	Fisher scientific	99.1%	Electrolyte solution
Acetone	Pharmaco-AAPER		Cleaning substrates
ITO glass substrates	Pilkington		Substrates
Scotch tape			Spacers

3.1 Procedure for sol-gel formation:

The basic method for the entire experimental design for the photo electrodes formation is very simple and represented in the following flow chart:

Chart-I:



3.2 Preparation of TiO₂ paste by using 4 different Approaches:

3.2.1 Approach I: In this method, TiO₂ paste is developed by using acid-base (acetic acid and ammonium hydroxide) chemistry. The TiO₂ paste prepared exhibits high viscosity, which enables the formation of thick TiO₂ films without requiring excessive thermal sintering [20]. After doing detailed investigation on the morphology of these films, which are processed at 150 °C, the films are recommended for all plastic-based/membrane based dye sensitized solar cells, which cannot be processed at high temperatures.

The viscosity of TiO₂ colloidal solution was found to increase, reaching a maximum at a certain point and then decreasing slightly upon addition of more ammonia solution.

A maximum viscosity of 5.3×10^4 cP was obtained near 5-wt% concentration of NH₃ (aq) with respect to TiO₂ [20]. It is remarkable that a change in viscosity as large as 3×10^4 cP was achieved when the pH of the pristine TiO₂ colloid was only slightly changed from 1.9 to 2.2. Further addition of ammonia decreased the viscosity because of an increase in total water content; in other words, the viscosity decreased due to a dilution effect. The reason for an increase in viscosity upon addition of ammonia to the TiO₂ colloid solution is likely to be related to flocculation of the nanoparticles (Flocculation is process of contact and adhesion whereby dispersed particles are held together by weak physical interactions ultimately leading to phase separation by formation of precipitates of larger than colloidal size). It is known that weak interparticle bonds in slurries of flocculated particles makes the slurry more viscous than a slurry of dispersed particles. Slurries can be dispersed or flocculated by changing pH, associated with the point of zero charge (pzc), and/or by adding suitable ions [21].

3.2.1.1 Procedure for preparing sol-gel in Approach I:

A volume of 37 mL of titanium (IV) isopropoxide (TTIP) (Aldrich, 99.9%) in 10 mL of 2-propanol was slowly dripped over a 30 min interval into a stirred mixture of 80 mL glacial acetic acid and 250 mL deionized water at 0 °C. The resulting solution was heated to 80 °C for 8 h in a hood. It was then heated to 230 °C for 12 h in a titanium autoclave (from Parr which is shown in the following figure). Upon removal from the autoclave, the solution was sonicated for 5 min with a ultra sonicator with an approximate power of 250 W. The solution was then concentrated to 150 g/L [22].

3.2.1.2 About the reactor and operating conditions during the sol-gel preparation:

- The vessel used in this reactor is completely made of titanium and it can withstand the pressure up to 600 psi.
- The titanium autoclave has built-in pressure gauge, a thermocouple and a stirrer through with which we can monitor the operating conditions by using 4848 Controller

which is shown in Figure 3.1.



Figure 3.1: Model 4544 High Pressure Reactor, 600 mL, Moveable Style Vessel, with heater lowered, and a 4848 Controller shown with optional Expansion Modules.

The temperature is ramped to 230 °C by 10 °C increments for every minute so that the pressure reaches to 400 psi. The entire experiment is done in nitrogen environment.

The binder free TiO₂ paste was prepared by adding 10 M ammonia solution, which is diluted from 28% conc. NH₄OH solution (14.8 M), to 10 g of 12.5% acidic TiO₂ colloidal solution while stirring. The amount of ammonia added with respect to the TiO₂ colloid solution was 5%.

3.2.2 Approach II:

This sol-gel procedure is similar to the one above, except this TiO₂ paste is prepared from (Degussa, Japan) P-25 TiO₂ (polymorphic i.e., includes all phases) powder instead of making it from the iso-propoxide.

3.2.3 Approach III:

In this sol-gel method the TiO₂ paste or solution is formed by adding an organic binder like diethanolamine (DEA) to alcoholic titanium isopropoxide solution. DEA suppresses the precipitation of oxides from the titanium isopropoxide solution during hydrolysis, so that much more water can be added to the Ti (O-i-Pr)₄-diethanolamine-i-propanol solution to give a clear solution. The dissolved organic binder is burned out during a high temperature sintering process at 500-600 °C.

3.2.3.1 Procedure for preparing sol-gel in Approach III:

In beaker I, a 5.0 g of titanium tetraisopropoxide is mixed with 20.5ml of isopropanol and kept aside. In beaker II 0.55 g of de-ionized water are mixed with 5.5 mL of isopropanol, both beakers and the binder (DEA) were taken into the glove box and purged with nitrogen gas. After purging with nitrogen gas, 4.26 g of DEA is weighed out and then slowly added to the beaker I, which contains TTIP and isopropanol while stirring for about 2 h. After this step slowly add the contents of beaker II to beaker I in order to prepare clear TiO₂ sol-gel. Now the sol-gel is ready for forming TiO₂ films.

3.2.4 Approach IV:

In this approach, the slurry of TiO_2 is prepared by simply adding the P-25 TiO_2 particle in water and then the TiO_2 solution is coated and sintered at high temperatures (450 to 600 $^{\circ}\text{C}$).

After preparing the TiO_2 sol-gel, the 1" x 1" ITO glass substrates (Pilkington) were cleaned in a sonicator for 15 minutes and with acetone and dried. All the sol-gel recipes prepared are coated on glass substrates by the doctor-blade technique and then dried at different temperatures depending upon the type of recipe selected. Doctor blade technique was a film smoothing method using any steel, rubber, plastic, or other type of blade to apply or remove a liquid substance from another surface. The term "doctor blade" is derived from the name of a blade used in conjunction with the ductor roll on a letterpress. The term "ductor blade" eventually mutated into the term "doctor blade." Based on the doctor blade method [23,24,25], the doctor blade used in this study employed a stainless steel blade to remove extra TiO_2 paste on the conductive side of the glass substrate, where the area is immobilized by 3M Scotch magic tape strips on it. Figure 3.2 shows the doctor blade method using squeegee to smooth the taped area [23].

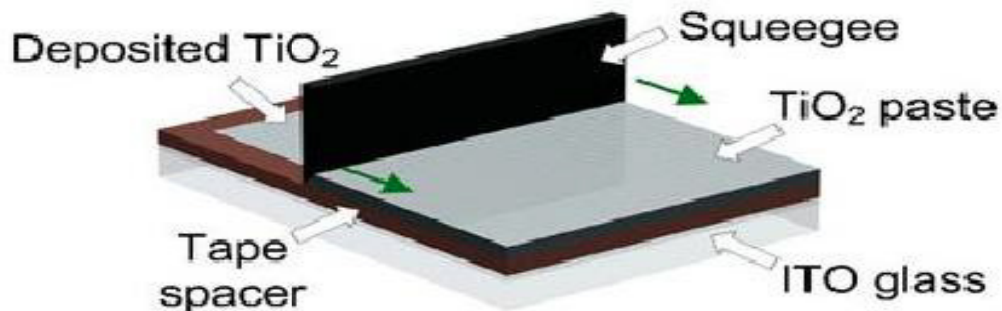


Figure 3.2: Doctor blade TiO_2 paste on ITO glass substrate with squeegee [23]

The 3M Scotch magic tape is used to create a one centimeter square area on a cleaned 1" x 1" ITO glass substrates. The 3M tapes are squeezed with a metal spatula to remove out air bubbles within the taped area. The TiO₂ paste is then added using a glass pipette placing it into the area. The doctor blade method is used to obtain a smooth paste surface. The ideal thickness of TiO₂ is approximately 10 microns [26]. Higher thickness of the film is able to ensure more dye loading for higher efficiency. However, there are trap states existing in the TiO₂ film, which will capture electrons and make it easier to recombine with electrolyte or oxide dye. When the thickness of the film increases, the possibilities of charge recombination also rise. On the other hand, if the thickness of the film is too thin, it will lower the dye loading which could affect adversely of the overall efficiency of the DSSC. In our research, we are measuring the photoactivity of TiO₂ film without any dye sensitization, so we selected an optimum thickness range from 10 to 40 microns. The prepared film is then kept at room temperature for low rate evaporation. Otherwise, the TiO₂ films will crack after drying in the oven at room temperature. When the film is dried, there should be no cracks in it and the film should not flake off from the glass substrate, either. If the cracks appear on the substrates then multiple coatings are performed until we achieve a uniform crack-less film. The following Table 3.2 gives the processing temperature for the sol-gels prepared.

Table 3.2: Processing temperature of different sol-gels

Processing temperatures	
Approach I	Initially dried at room temperature then sintered at 150 ⁰ C for 30 min
Approach II	Initially dried at room temperature then sintered at 150 ⁰ C for 30 min
Approach III	Dried at 100 ⁰ C for 24 h than sintered at 600 ⁰ C for 30 min
Approach IV	Initially dried at room temperature then sintered at 150 ⁰ C for 30 min

Chapter 4

4. Techniques used for film characterization:

4.1 Thermogravimetric Analysis (TGA)

After film formation, the decomposition reactions and chemistry involved can be investigated by using a technique known as Thermogravimetric analysis (TGA). The instrument is connected to nitrogen tank to have a dry and inert atmosphere in the sample holder during the entire experimental operation.

The TGA instrument mainly consists of 3 parts, a high temperature furnace, a sample holder, and a balance. Changes in weight occur when the sample begins to decompose, and these changes are recorded and represented as a thermogram. During TGA, a minimum temperature is normally chosen such that the weight of the specimen remains stable and all chemical reactions occurring go to completion. In principle, a sample of the test material is placed into a alumina cup that is supported on or suspended from an analytical balance located outside the furnace chamber. The balance sends the

weight signal to the computer for storage, together with the sample temperature and the time transpired. The TGA curve plots the signal that is already converted to percent weight change on the Y-axis against the reference material temperature on the X-axis [27]. The instrument used in our research is TA Instruments 2050 TGA.

4.2 Differential scanning calorimetry (DSC):

A DSC instrument has four important components: heater, sample pan, reference pan, and heat detectors. The sample pan is used to hold the sample, while the reference pan is left empty. Each pan sits on top of a heater, and a computer program is used to control the heating rate at around 5 degrees per minute. The chosen heating rate stays constant through out the experiment. The computer program ensures that the two separate pans are heated at the same rate. It is important to note that if there were no controlled heating, the two pans would not heat at the same rate. This is due to one pan having a sample and the other being empty. Since we have extra material in the sample pan, it will take more heat to keep the temperature of the sample pan increasing at the same rate as the reference pan. The heater underneath the sample pan has to work harder than the heater underneath the reference pan. In a DSC experiment, it is measuring more heat than the sample pan is putting is consuming [27]. The instrument we used in our research is a TA Instruments 2910 DSC.

4.3 Attenuated Total Reflectance FT-IR spectroscopy:

Infrared spectroscopy exploits the fact that molecules have specific frequencies at which they rotate or vibrate corresponding to discrete energy levels (vibrational modes). These resonant frequencies are determined by the shape of the molecular potential energy surfaces, the masses of the atoms, and the associated vibronic coupling. In order for a

vibrational mode in a molecule to be IR active, it must be associated with changes in the permanent dipole.

Simple diatomic molecules have only one bond, which may stretch. More complex molecules have many bonds, and the vibrations can be conjugated, leading to infrared absorptions at characteristic frequencies that may be related to chemical groups. Examination of the transmitted light reveals how much energy was absorbed at each wavelength. Analysis of these absorption characteristics reveals details about the molecular structure of the sample.

ATR uses a property of total internal reflection called the evanescent wave. A beam of infrared light is passed through the ATR crystal in such a way that it reflects at least once off the internal surface in contact with the sample. This reflection forms the evanescent wave, which extends into the sample, typically by a few micrometers. The beam is then collected by a detector as it exits the crystal. This evanescent effect works best if the crystal is made of an optical material with a higher refractive index than the sample being studied. In the case of a liquid sample, pouring a shallow amount over the surface of the crystal is sufficient. In the case of a solid sample, it is pressed into direct contact with the crystal. Because the evanescent wave into the solid sample is improved with a more intimate contact, solid samples are usually firmly clamped against the ATR crystal, so that trapped air is not the medium through which the evanescent wave travels, as that would distort the results.

4.4 X-ray fluorescence spectroscopy:

X-ray spectroscopy is based on measurement of emission, absorption, scattering, fluorescence, and diffraction of electromagnetic radiation in the X-ray wavelength region.

X-ray fluorescence and X-ray absorption methods are widely used for the quantitative and qualitative determination of all elements in the periodic table having atomic numbers greater than that of boron, depending on the instrument used. The S2 Ranger X-ray fluorescence instrument used in the current studies can detect elements Na and Mg or up.

4.4.1 Basic theory and principle involved:

X-rays are short wavelengths of electromagnetic radiation that can be produced by the electronic transitions of electrons in the inner orbitals of atoms. When a primary x-ray from e.g. an x-ray tube or a radioactive source strikes a sample, the x-ray can either be absorbed by atoms of the material or scattered by the material. The process in which an x-ray is absorbed by an atom by transferring all of its energy to an innermost electron is called the "photoelectric effect." Each element has electronic orbitals of characteristic energy. Following removal of an inner electron by an energetic photon provided by a primary radiation source, an electron from an outer shell drops into its place. The main transitions are given names: an L→K transition is called K alpha, an M→K transition is called K beta, and M→L transition is called L alpha and so on. (These transitions are shown in the Figure 4.1) Each of these transitions yields a fluorescent photon with a characteristic energy equal to the difference in energy of the initial and final orbital. The wavelength of this fluorescent radiation can be calculated from Planck's law

$$\lambda = h c/E$$

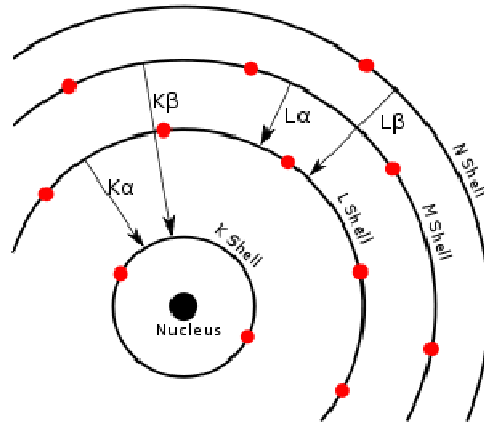


Figure 4.1: Core electronic transitions in an atom

Absorption of an x-ray quantum causes ejection of the innermost electrons from an atom and the consequent production of an excited ion. In this process the entire energy $h\nu$ of the radiation is portioned between the kinetic energy of the electron and the potential energy of the excited ion. The highest probability of absorption arises when the energy of the quantum is exactly equal to the energy required to remove the electron just to the periphery of the atom.

4.5 Powder X-ray diffraction method:

4.5.1 Theory and background:

In 1912 Max von Laue discovered that crystals act as three dimensional diffraction gratings for X-ray radiation with wavelengths similar to the spacing of planes in a crystal lattice and it was later discovered that it is based on constructive and destructive interference of monochromatic X-rays passing through a crystalline sample. In our experiment, X-rays were produced using a copper anode ray tube, filtered to produce monochromatic radiation (in this case Cu K-alpha radiation), collimated to straighten them and directed toward the sample. Unlike single crystal x-ray diffraction,

the samples under analysis were polycrystalline. In the presence of many single crystals put together to form a polycrystalline material, some crystals are always in diffraction condition for every Θ angle, and instead of individual diffraction spots as in single crystal diffraction rings of diffracted intensity at a certain Θ angle are obtained that correspond to the d spacing for an atomic plane with the Miller indices (hkl) . Using the powder method, TiO_2 is ground up to a fine powder and in this powder we obtain thousands of grains that have random orientations. With random orientations we might expect most of the different atomic planes to lie parallel to the surface in some grains. Thus by scanning through an angle Θ of incident x-ray beams from 0° to 90° we could expect to find all the angles where diffraction has occurred, and each of these angles would be associated with a different atomic spacing. The goniometer keeps the track of angle Θ and sends the information to a computer, while the detector records the x-rays coming out the other side of sample and sends this information to the computer. The angle 2Θ for each diffraction peak can then be converted to d -spacing, using the Bragg equation shown below.

$$n\lambda = 2d\sin \Theta$$

One can then work out the crystal structure and associate each of the diffraction peaks with a different atomic plane in terms of the Miller index for that plane $(h k l)$. There exist databases in which data has been collected on thousands of crystalline substances. Since every compound with the same crystal structure will produce an identical powder diffraction pattern, the pattern serves as kind of a 'finger print' for the substance, and thus comparing an unknown mineral to those in the powder diffraction file enables easy identification of an unknown.

4.5.2 Instrumentation principle:

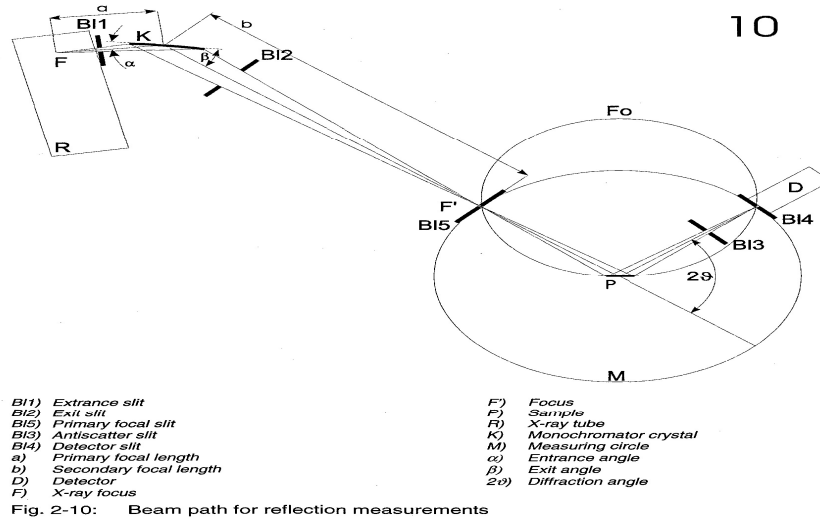


Figure 4.2: Powder X-ray diffraction instrumentation

A sample should exhibit a plane of flattened surface. The angle of both the incoming and exiting beam is θ with respect to the specimen surface. The diffraction pattern is collected by varying the incident angle of incoming x-ray beam by θ and the scattering angle by 2θ while measuring the scattered intensity $I(2\theta)$ as a function of latter. Two angles have to be varied during a $\theta/2\theta$ scan and various types of powder diffractometers are in use. For one set of instruments, the x-ray source remains fixed while the sample is rotated around θ and detector moves by 2θ . For other systems the sample is fixed while both x-ray source and detector rotate by θ simultaneously, but clockwise and counter clockwise respectively. The rotations are performed by a goniometer, which is the central part of a diffractometer. A goniometer of a powder diffractometer comprise of at least two circles or equally two axes of rotation. Typically the sample is mounted on the rotational axis, while detector and/or x-ray move along the periphery, but both axes of rotation coincide. In most laboratories $\theta/2\theta$ diffractometers, the goniometer radius,

which is the sample to detector distance, is in the range 150-500 mm. Highly precise goniometers with 0.001° precision and even lower on both the Θ and 2Θ circles of $2\Theta_i$ positions and a second vector with appropriate intensities I_i . The step size $\Delta 2\Theta_i$ between two adjacent $2\Theta_i$ should be chosen with the intended purpose of data. For chemical phase analysis, full width at half maximum of the tallest Bragg peak in the pattern should be covered at least 5 to 7 measurement points. However, for a microstructural analysis, an excess of 10 points should be measured on the same scale. The appropriate value of $\Delta 2\Theta_i$ will also depend on the slit configuration of diffractometer. The preset integration time of the detector per step of $2\Theta_i$ should allow the integral intensity of small peaks of interest to exceed the noise fluctuations $\sigma(I)$ by a factor of 3 or 5 or other values according to the required level of statistical significance. The control of the X-ray beam bundle suffers from the constraints of the lenses and other refractive elements, which are not as easily applied as used for visible light. For this reason the beam conditioning in $\Theta / 2\Theta$ diffractometers is mostly performed by slits and apertures and, may be termed shadow casting optics.

4.6 Scanning electron microscopy (SEM):

The scanning electron microscope (SEM) is an instrument capable of producing high-resolution images of a sample surface at large magnification not achievable with optical microscopy. SEM images have a characteristic three-dimensional appearance and are useful for judging the surface morphology of the sample.

The scanning electron microscope (SEM) uses a focused beam of high-energy electrons to generate a variety of signals at the surface of solid specimens. The signals that derive from electron-sample interactions reveal information about the sample

including external morphology (texture), chemical composition, and crystalline structure and orientation of materials making up the sample. In most applications, data are collected over a selected area of the surface of the sample, and a 2-dimensional image is generated that displays spatial variations in these properties. Areas ranging from approximately 1 cm to 5 microns in width can be imaged in a scanning mode using conventional SEM techniques (magnification ranging from 20X to approximately 30,000X, spatial resolution of 50 to 100 nm). The SEM is also capable of performing analysis of selected point locations on the sample; this approach is especially useful in qualitatively or semi-quantitatively determining chemical compositions (using Energy-Dispersive X-Ray Spectroscopy, EDS), crystalline structure, and crystal orientations (using Electron Backscatter Diffraction EBSD). The instrument we used in our research is JEOL JIB-4500 focused ion beam system.

4.6.1 Working Principle:

The working principle in SEM is very simple; it mainly uses a beam of electrons, which are emitted thermionically from a tungsten or lanthanum hexaboride (LaB_6) cathode and are accelerated towards an anode. Tungsten is used because of its high melting point and low vapor pressure, thereby allowing it to be heated for electron emission. The electron beam, which typically has an energy ranging from a few hundred eV to 100 KeV, is focused by one or two condenser lenses into a beam with a very fine focal spot, sized 0.4 nm to 5 nm. Then the beam passes through pairs of scanning coils or pairs of deflector plates in the electron optical column, typically in the objective lens, which deflects the beam horizontally and vertically so that it scans in a raster fashion over a rectangular area of the sample surface. When the primary electron beam interacts with the sample,

the electrons lose energy by repeated scattering and absorption within a teardrop-shaped volume of the specimen known as the interaction volume, which extends from less than 100 nm to around 5 μm into the surface. The size of the interaction volume depends on the electrons' landing energy, the atomic number of the specimen and the specimens' density. The energy exchange between the electron beam and the sample results in the emission of electrons and electromagnetic radiation, which can then be detected to produce an image.

4.7 Electrochemistry and Photovoltaic measurements:

Redox properties were determined via electrochemical methods. Cyclic voltammetry (CV) is the most versatile electroanalytical technique for the study of electroactive TiO_2 photoanodes. The effectiveness of CV results from its capability for rapidly observing the redox behavior over a wide potential range. The voltammogram produced is a display of current (vertical axis) versus potential (horizontal axis). As the potential varies linearly with time, the horizontal axis can also be thought of as a time axis [28]

Cyclic voltammetry requires a waveform generator to produce the excitation signal, a potentiostat to apply this signal to an electrochemical cell, a current-to-voltage converter to measure the resulting current, and some means of displaying the voltammogram. The potentiostat insures that the working electrode potential will not be influenced by the reactions which take place.

The cyclic voltammetry used for our analysis was performed on a potentiostat/galvanostat model 273A (Parr). A three-electrode cell was used which consisted of a platinum wire counter electrode and a Ag/AgCl reference electrode, TiO_2

photo anode as working electrode. The electrolyte solution is 0.1N NaOH. The light source we used is Newport solar simulator, which has Xenon lamp and operated at AM1.5 conditions.

Chapter 5

5. Results and discussion:

5.1 Thermal decomposition of TiO₂ sol-gel prepared from Approaches I and II:

A 6.241 mg of anhydrous ammonium acetate was transferred into aluminum TGA pan and run as a reference sample after flushing the TGA instrument with nitrogen gas for 5 min. Then 15 to 20 mg of our TiO₂ gel was then analyzed using the same method and experimental parameters. Experimental parameters and results are shown in the following Figures 5.1, 5.2 and 5.3:

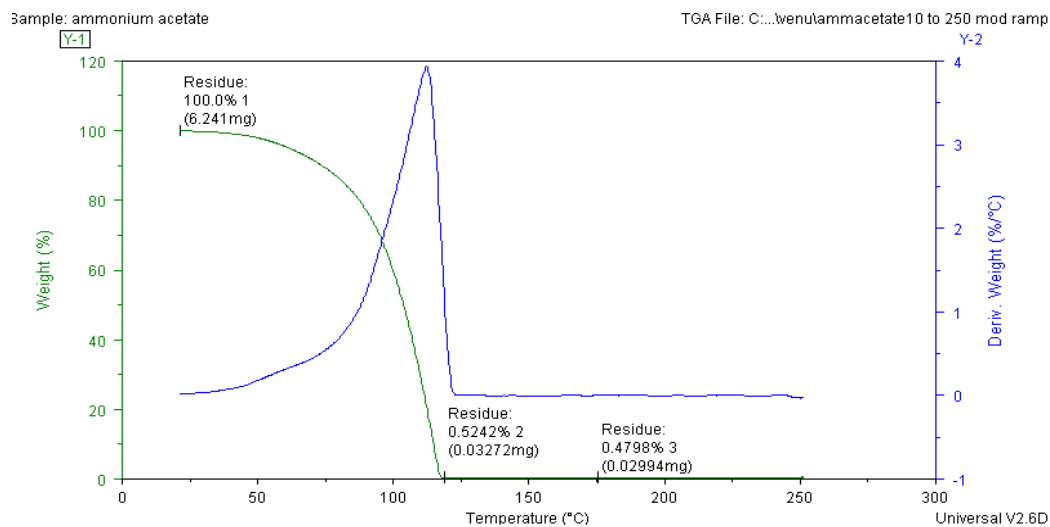


Figure 5.1: TGA thermogram of anhydrous ammonium acetate.

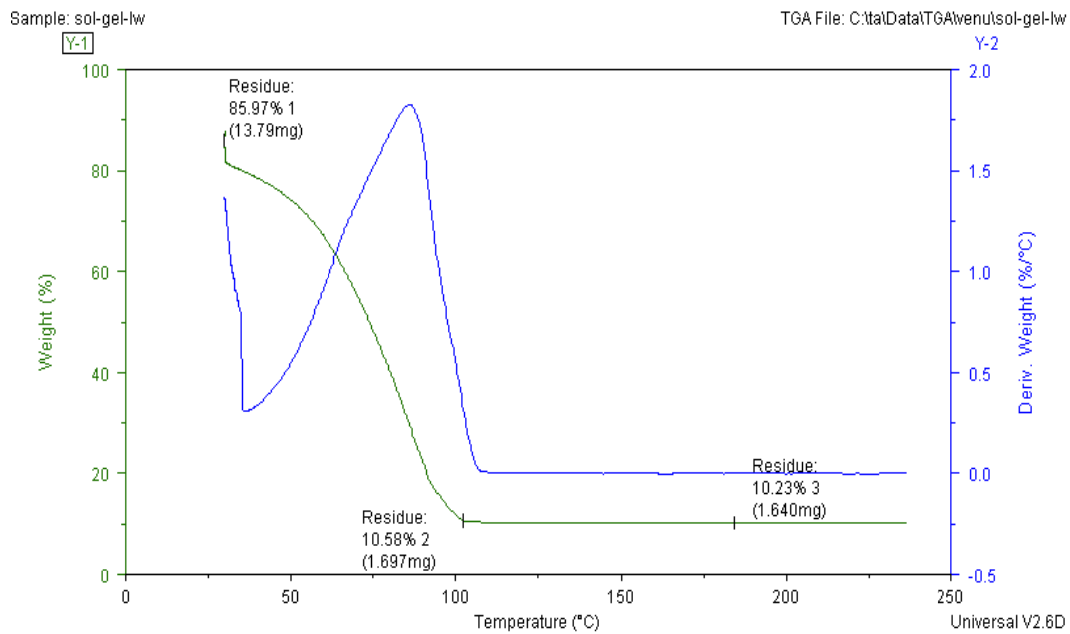


Figure 5.2: TGA thermogram of unsintered TiO_2 gel prepared from Approach I

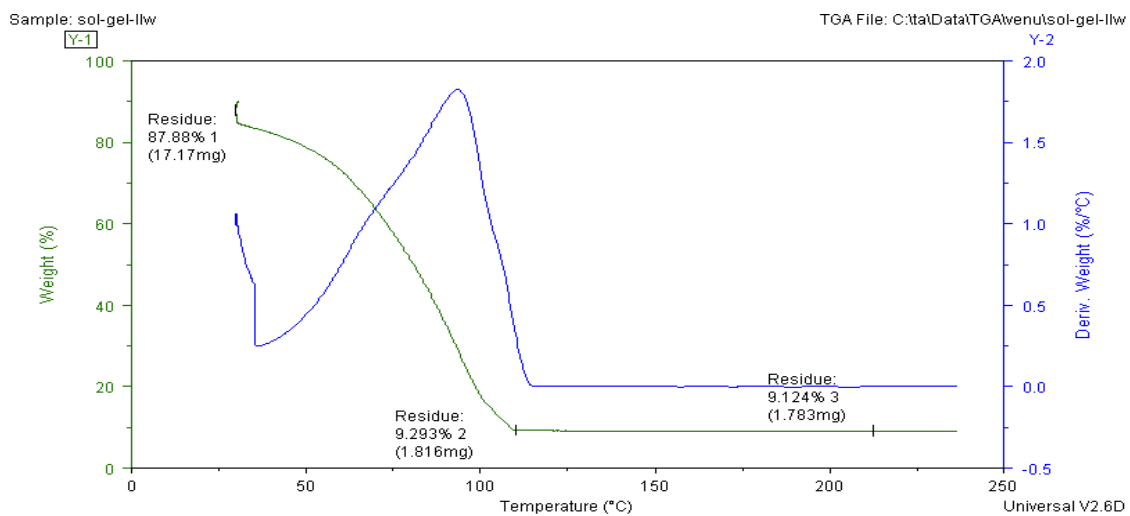


Figure 5.3: TGA thermogram of unsintered TiO_2 gel prepared from Approach II

Table 5.1: Method and experimental parameters for sol-gel prepared from Approaches I and II

Name	Sample size	Method
Ammonium acetate	6.241 mg	• Ramp 10 °C per min up to 250 °C
TiO ₂ Sol-gel prepared from Approach I	15.0040mg	• Ramp 10 °C per min up to 250 °C
TiO ₂ Sol-gel prepared from Approach II	19.5380mg	• Ramp 10 °C per min up to 250 °C

The thermograms shown in the above Figures 5.1, 5.2 and 5.3 have a single significant weight loss step and corresponds to a weight loss of 99.48%, 89.42% and 90.71% from the original weight, respectively. The weight loss in Figures 5.2, and 5.3 is associated with water and solvent loss. However these samples were analyzed in a gel form, which contains both water and other solvent mixtures, like ammonia, acetic acid and a complex salt formed between these two. Ammonium acetate starts decomposing at ~114 °C, water and acetic acid evaporates at 100 °C and 118 °C, so this weight loss corresponds to ammonium acetate, water and acetic acid loss.

5.2 Thermal decomposition of TiO₂ sol-gel prepared from Approach III:

The TGA instrument was again flushed with nitrogen gas in the same way as in our previous experiments for sol-gels prepared from Approaches I and II. A sample size of

about 18.95 mg was quickly transferred into the aluminum TGA pan and the pan was mounted into the furnace. The experimental parameters and results are shown in the following Table 5.2 and Figure 5.4:

Table 5.2: Method and experimental parameters for sol-gel prepared from Approach III

Name	Sample size	Method
TiO ₂ sol-gel prepared from Approach III	18.95 mg	<ul style="list-style-type: none"> Ramp 10 °C per min up to 500 °C

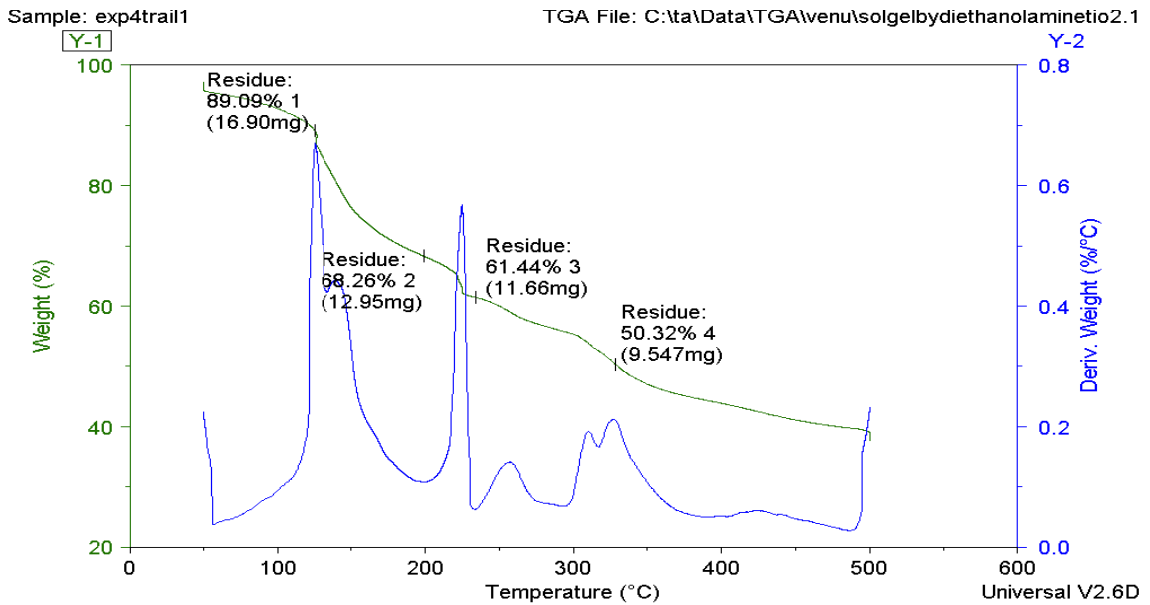


Figure 5.4: TGA thermogram of unsintered TiO₂ sol-gel prepared from Approach III.

The sol-gel prepared from Approach III was from conventional protocol which includes an organic binder such as diethanolamine (DEA), which helps the TiO₂ particles to bind to the substrate.

The thermogram shown in Figure 5.4 has four decomposition steps. The first step corresponds to a weight loss of about 10.91% from original weight. This weight loss is due to an equilibration step; the sample is adjusted to furnace temperature and in the process small amounts of water and other liquid constituents are lost. The reaction mixture in this method includes water, isopropyl alcohol, DEA and TTIP. The second and third decomposition steps correspond to a weight loss of 28.83% and 6.82%, respectively. This is due to the evaporation of DEA, since boiling point of DEA is ~ 217 °C, leaving TiO_2 particles on the substrate. The fourth decomposition step corresponds to a weight loss of 11.12 and is associated with decomposition of TTIP. TTIP disassociates into $\text{Ti}(\text{OH})_4$ and isopropyl alcohol, later $\text{Ti}(\text{OH})_4$ dehydrates to TiO_2 and water. [29].

The thermogram in Figure 5.5 shows the overlay of all three sol-gel form different Approaches.

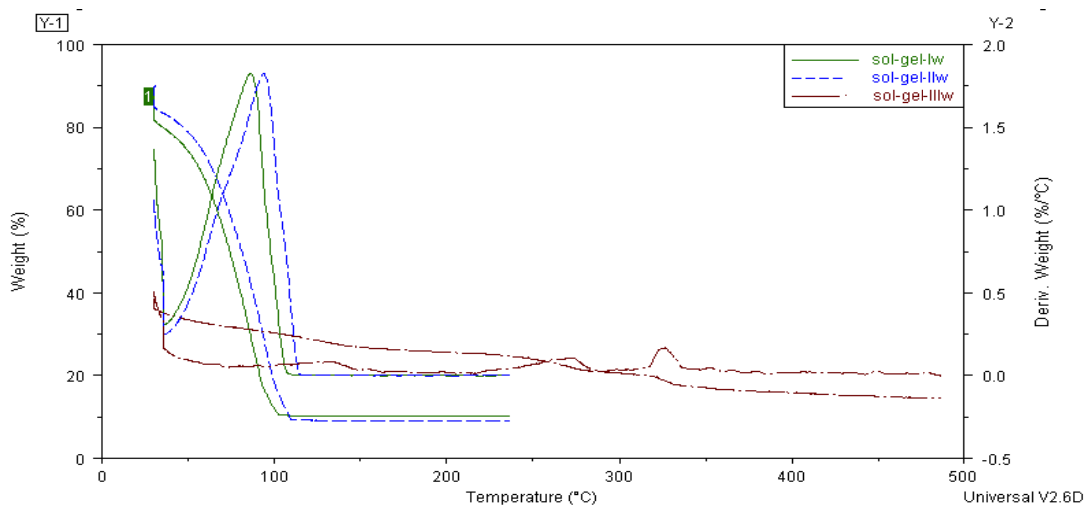
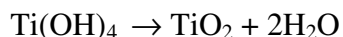
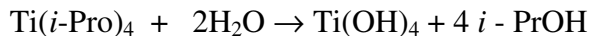


Figure 5.5: Overlay of TGA thermograms of unsintered TiO_2 gels prepared from Approaches I, II and III

Overall, the TGA data of sol-gels prepared from Approaches I and II indicate that TiO₂ film formation proceeds in single characteristic step. This step occurs at 110 °C, which was acknowledged to loss of complex salt formed from acetic acid and ammonia.

The TGA data for the sol-gel prepared from approach III was different when compared with the other two. This was because of the reactants used in this approach; it contains an organic binder (DEA). The thermogram for this sol-gel (Figure 5.4) had four corresponding decomposition steps. The first step occurs at 25 °C, and was attributed to equilibration of sample with furnace temperature. Second and third steps occurred at a temperature range of 200 - 230 °C, which correspond to evaporation of DEA, and the final step is at 320 °C, which is associated with cleavage of TTIP to TiO₂ and water molecules. After the sintering process the substrate is left over with TiO₂ film.



5.3 Analysis of DSC thermograms:

In order to confirm the above decomposition steps, the sample was analyzed by using Differential Scanning Calorimetry. The sol-gel prepared from Approach I is our challenging task. Thus the sol-gel sample size of 1.9690 mg was collected and transferred in the aluminum DSC pan and crimped with the lid to form a DSC sample pellet. Simultaneously, an empty sample pan is also prepared to correct the background. The weight of the sample is measured by using the balance in the TGA instrument, which is 1.969 mg. Before running the sample, the instrument is flushed with dry nitrogen gas and

then the sample is loaded into the chamber and sealed with a glass dome. The results are explained in the Figure 5.6

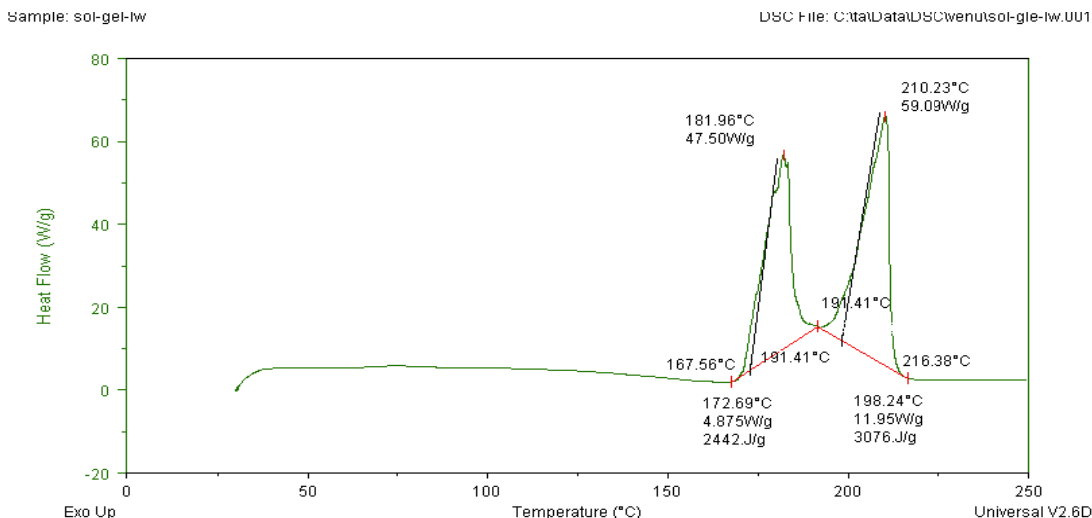


Figure 5.6: Transitions occurring in DSC curve of unsintered TiO₂ gel prepared from approach I.

Based on the DSC curve, the transitions occurred at 181.96 °C and 210.23 °C. The transitions at 181.96 °C and 210.23 °C correspond to melting point and decomposition of complex salts formed from the reaction of ammonium hydroxide, acetic acid and TiO₂. Pure ammonium acetate melts at 114 °C and later it decomposes and this was confirmed by performing TGA and DSC of ammonium acetate as reference sample. But we observed the activity at 181.96 °C and 210.23 °C and this is due to the formation of a complex salts between the initial reactants.

5.4 Interpretation of sol-gel samples by IR spectroscopy:

After sintering the sol-gel samples, the viscosity agents (acetic acid, ammonium acetate and water) should have been evaporated completely. In order to confirm that ammonium acetate and other organics have been completely evaporated, infrared spectroscopic analysis was employed. Ammonium acetate was run as a reference. The sol-gel samples

prepared from Approaches I, II and III were also analyzed in both unsintered and sintered conditions for confirming that these compounds are absent. The subsequent spectrum in the Figures 5.7, 5.8, 5.9, 5.10, 5.11 and 5.12 clearly shows that all the solvent has been evaporated completely.

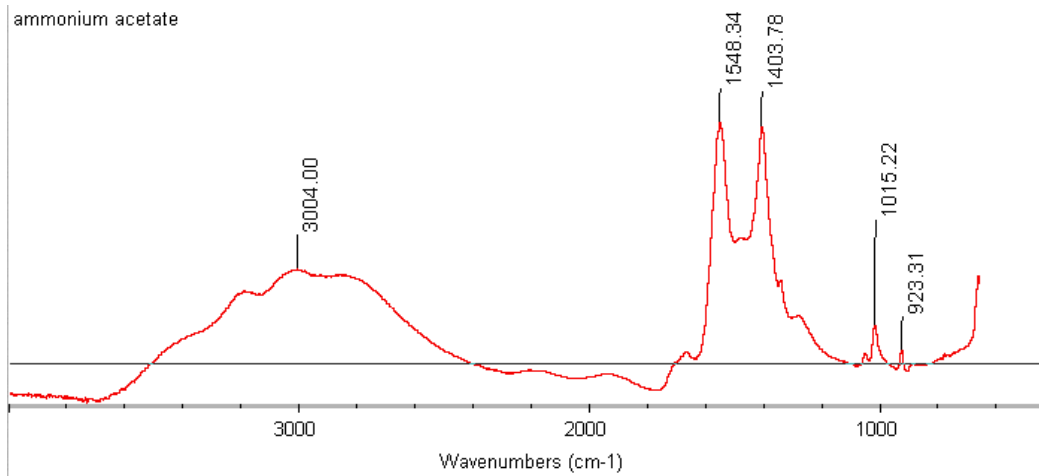


Figure 5.7: IR spectrum of ammonium acetate

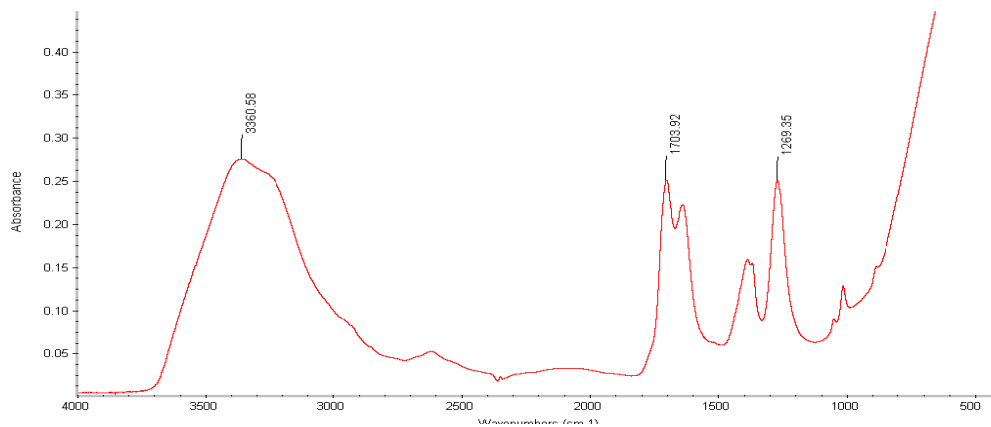
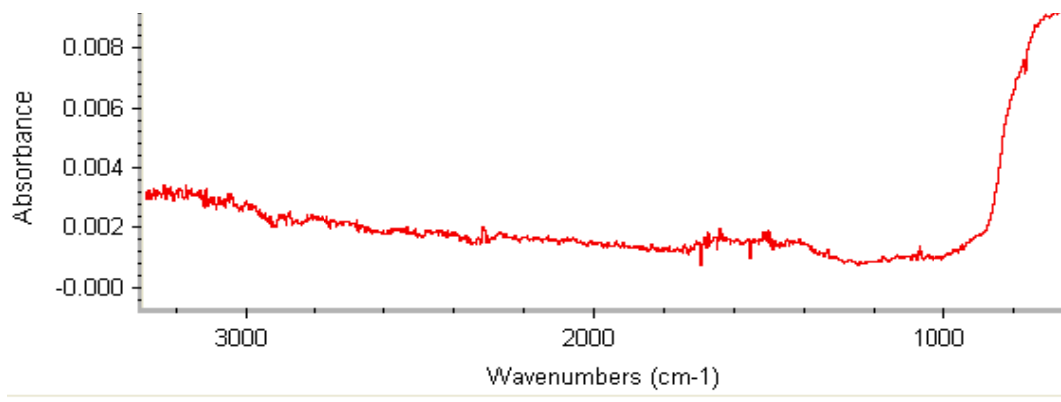


Figure 5.8: IR spectrum of unsintered TiO₂ gel prepared from Approach-I



sol-gel-I

Figure 5.9: IR spectrum of sintered TiO₂ gel prepared from Approach-I

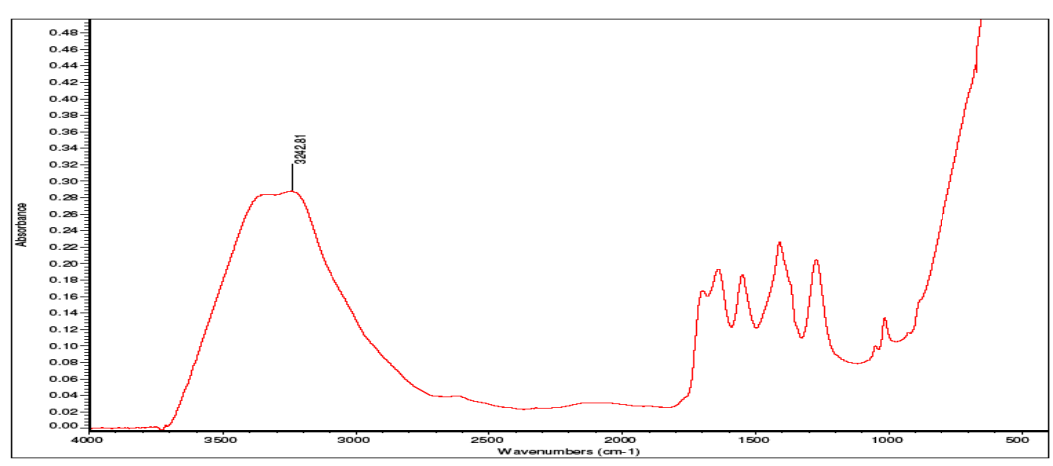


Figure 5.10: IR spectrum of unsintered TiO₂ gel prepared from Approach-II

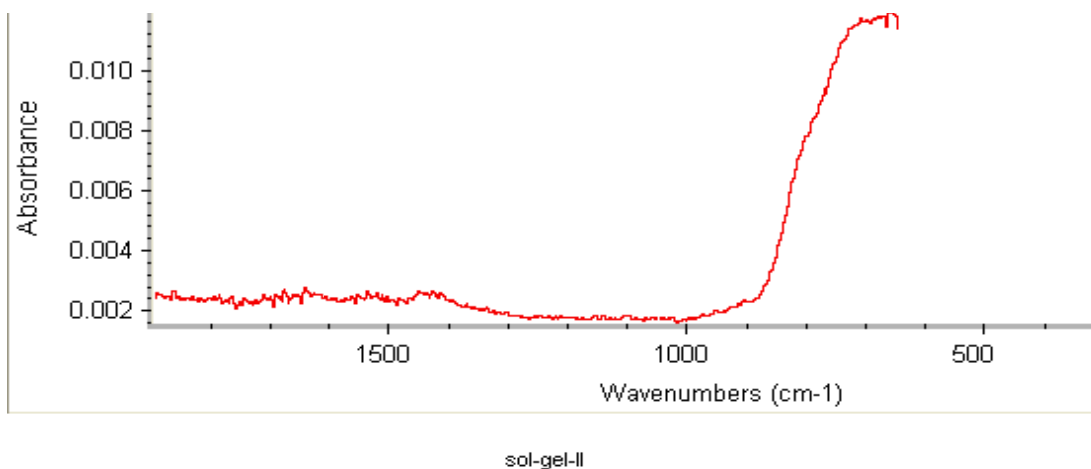


Figure 5.11: IR spectrum of sintered TiO_2 gel prepared from Approach-II

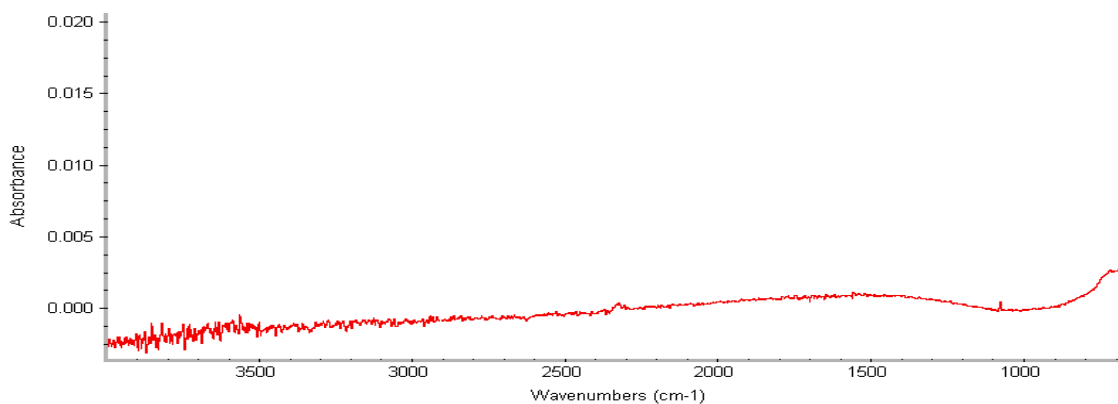


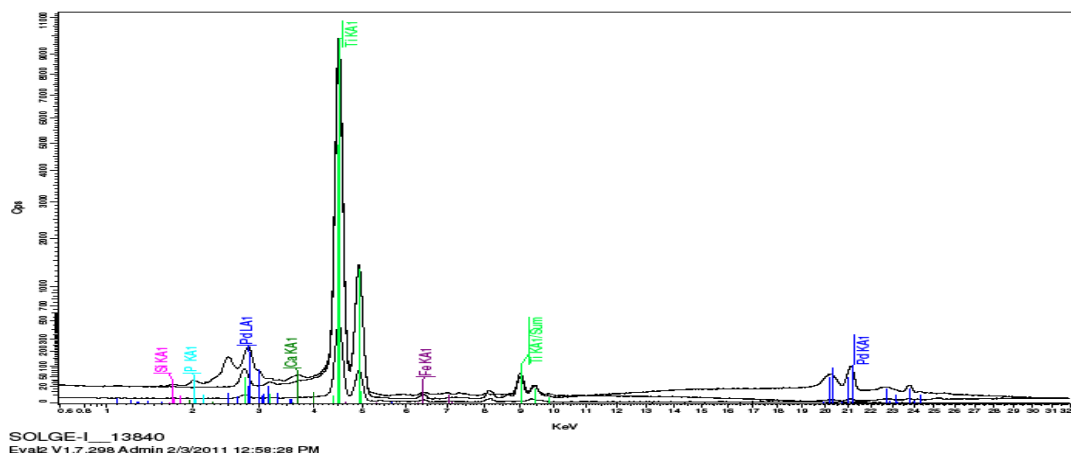
Figure 5.12: IR spectrum of unsintered TiO_2 gel prepared from Approach-III

An anhydrous ammonium acetate sample was run on infrared spectrometer and peaks were observed at 923.1, 1015.22, 1403.78, 1548.34 and 3004.00 cm^{-1} . The sol-gel samples obtained through Approaches I, II & III were observed under Infrared and no peaks were observed except for a single peak at 700 cm^{-1} , which corresponds to TiO_2 IR absorption [30]. This is evident from the Figures 5.8, 5.9, 5.10, 5.11 and 5.12. This clearly shows that the initial reactants acetic acid and ammonium hydroxide were completely evaporated during the sintering process and no traces were left in the final product. This is confirmed by the absence of peaks at the 923.1, 1015.22, 1403.78,

1548.34 and 3004.00 cm^{-1} , which was clearly evident in the infrared graph of ammonium acetate.

5.5 X-ray Fluorescence spectroscopic analysis of TiO_2 sol-gels prepared from approaches I, II & III:

The sintered TiO_2 films were scraped from the substrate surface and appropriate amounts of sample are transferred in to the XRF cup with Mylar film. Before running our samples, the instrument was calibrated by using a copper calibration disk, and then the collected sample is crushed in a clean mortar and then transferred into the cup. After loading the sample, the Mylar film application was selected for powder elemental analysis. The X-ray source and the detector used in this study is Pd X-ray source and Si-drift detector. The results of our films prepared are shown in the Figures 5.13, 5.14, 5.15, and 5.16.



Eval2 - [Quant] - [SOLGE-I_13840:2]

File View Quanti Window Tools Help

Active sample: SOLGE-I_13840

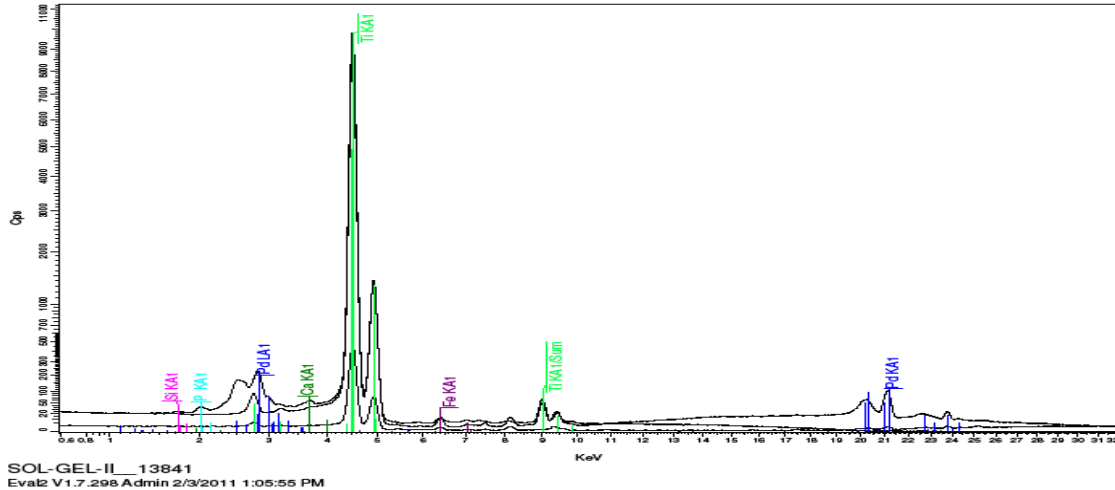
Sum:

Formula	Z	Concent...	Status	Line 1	Line ene...	Line 2	Line ene...	Line 3	Line ene...
Sample ...		0.04	Input						
Si	14	0.701 %	Fit spectrum	Si KA1...	1.7400	Si KA1...	1.7400	Si KA1...	1.7400
P	15	0.527 %	Fit spectrum	P KA1...	2.0137	P KA1...	2.0137		
Ca	20	1.042 %	Fit spectrum	Ca KA...	3.6918	Ca KA...	3.6918	Ca KA...	3.6918
Ti	22	97.685 %	Fit spectrum	Ti KA1/...	4.5110	Ti KA1/...	4.5110	Ti KA1/...	4.5110
Fe	26	0.045 %	Fit spectrum	Fe KA...	6.4041	Fe KA...	6.4041	Fe KA...	6.4041

Figure 5.13: XRF spectra showing elements in TiO₂ sol-gel sample prepared from Approach I

The sample was then quantitatively analyzed to assign the peaks by using software “spectra EDX”. We observed an intense peak at 4.5110 KeV, which corresponds to 97.685% Ti. It also had a sum peak at 9 KeV. Sum peaks occur due to a phenomenon where two X-rays essentially impact the detector instantaneously; thus the pulse created is measured as a sum of energies of two X-rays. In our sample we have mainly Ti (Ka1 of 4.5110 KeV) and thus the sum peak occurred at 9 KeV. The Mylar film that we used had trace amounts of calcium Ca and phosphorus P thus the peaks at 2.0137 KeV and 3.6918 KeV correspond to P and Ca elements from Mylar film. Even though our reactor is

completely made of titanium, a negligible amount of (0.045%) of iron Fe can be seen, which might be from the water, glassware or from a rusty stainless steel fitting we used. Si K α , Pd L α , Pd K α peaks at 1.7400 Kev, 2.85 Kev and 21.86 Kev are due to the source and detector we used.



Eval2 - [Quant] - [SOL-GEL-II_13841:2]

File View Quanti Window Tools Help

Active sample: SOL-GEL-II_13841

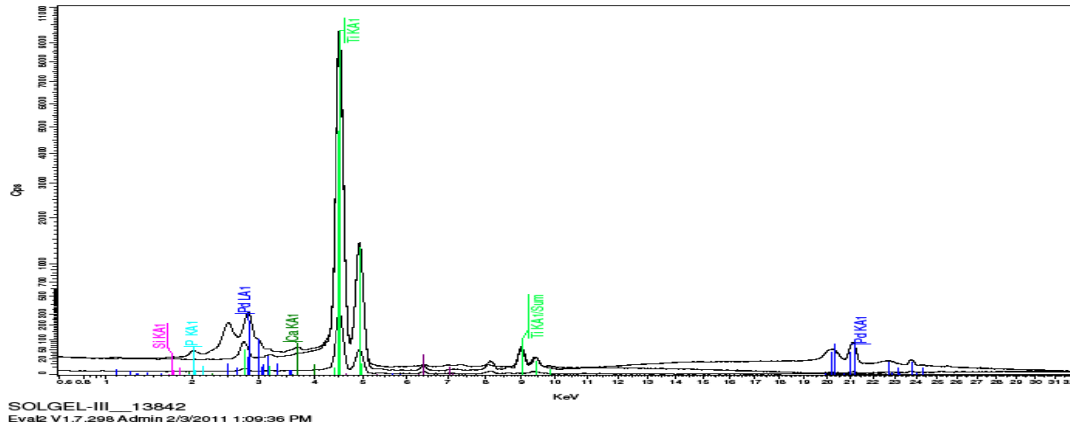
Sum:

Formula	Z	Concent...	Status	Line 1	Line ene...	Line 2	Line ene...	Line 3	Line ene...
Sample ...		0.04	Input						
Si	14	0.993 %	Fit spectrum	Si KA1...	1.7400	Si KA1...	1.7400	Si KA1...	1.7400
P	15	0.597 %	Fit spectrum	P KA1...	2.0137	P KA1...	2.0137		
Ca	20	1.174 %	Fit spectrum	Ca KA...	3.6918	Ca KA...	3.6918	Ca KA...	3.6918
Ti	22	97.107 %	Fit spectrum	Ti KA1/...	4.5110	Ti KA1/...	4.5110	Ti KA1/...	4.5110
Fe	26	0.130 %	Fit spectrum	Fe KA...	6.4041	Fe KA...	6.4041	Fe KA...	6.4041

Figure 5.14: XRF spectra showing elements in TiO₂ sol-gel sample prepared from Approach II.

The TiO₂ sol-gel sample prepared from Approach II is similar to Approach I, The only difference is the starting material. The TiO₂ sol is prepared from Degussa P-25 TiO₂. XRF analysis of this sample is mostly identical to approach I. The main peak in this

sample occurred at 4.5110 Kev and the sum peak at 9.0 Kev. Thus the sample has mostly Titanium and the result was identical to the sol-gel prepared from Approach I.



Eval2 - [Quant] - [SOLGEL-III_13842:2]

File View Quanti Window Tools Help

Active sample: SOLGEL-III_13842

Sum:

Formula	Z	Concent...	Status	Line 1	Line ene...	Line 2	Line ene...	Line 3	Line ene...
Sample ...		0.04	Input						
Si	14	1.263 %	Fit spectrum	Si KA1...	1.7400	Si KA1...	1.7400	Si KA1...	1.7400
P	15	0.984 %	Fit spectrum	P KA1...	2.0137	P KA1...	2.0137		
Ca	20	0.794 %	Fit spectrum	Ca KA...	3.6918	Ca KA...	3.6918	Ca KA...	3.6918
Ti	22	96.925 %	Fit spectrum	Ti KA1/...	4.5110	Ti KA1/...	4.5110	Ti KA1/...	4.5110
Fe	26	0.033 %	Fit spectrum	Fe KA...	6.4041	Fe KA...	6.4041	Fe KA...	6.4041

Figure 5.15: XRF spectra showing elements in TiO₂ sol-gel sample prepared from Approach III.

The TiO₂ sol-gel prepared from Approach III is the conventional high temperature sintering process. The main peak in this sample occurred at 4.5110 Kev and a sum peak at 9.0 Kev. The binder DEA used to adhere the particles is burned out during the sintering process, leaving TiO₂ film on the substrate. Thus the XRF analysis of the sample shows that our TiO₂ sol-gels prepared were pure and good for photovoltaic applications.

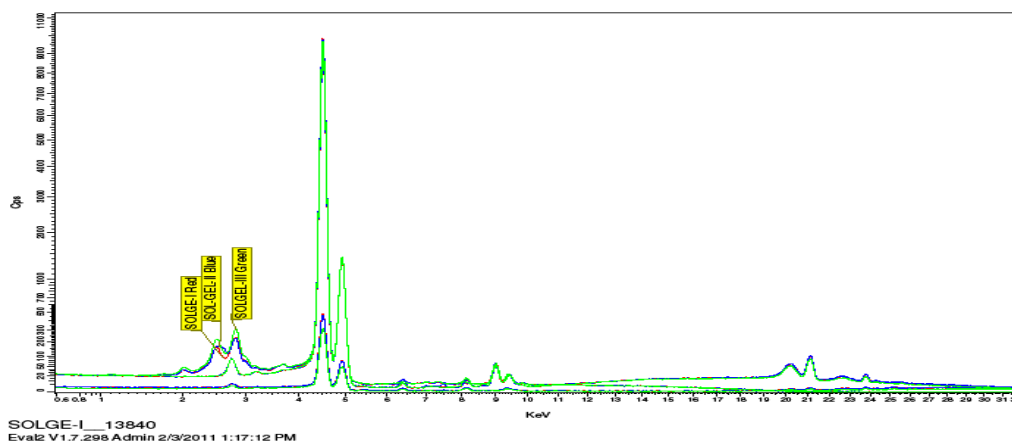


Figure 5.16: Overlay of XRF spectra showing the elements in TiO_2 sol-gel samples prepared from Approaches I, II and III.

After analyzing all the samples with spectra EDX, it was seen that the low temperature sol-gel formulations contain at least 97% of TiO_2 and they are identical to the sol-gels prepared by conventional process, which is Approach III. Figure 5.16 is an overlay of all the sol-gel samples prepared, which basically shows that we achieved a good result in preparing pure TiO_2 sol-gel without using any organic binder. However the particle size and shape are important to characterize a good photoelectrode; these attributes can be answered by performing XRD analysis.

5.6 XRD analysis for particle size and shape determination:

Powder X-ray diffraction analysis was performed in order to determine the crystal phase and particle size of the TiO_2 sol-gel sample. The instrument, which we used in this study is the D8 Advance Bruker diffractometer with Bragg Brentano geometry, and is explained in the Experimental section. The source and the detector we used is a Cu source and Vantech detector. X-ray diffraction method we used is non-destructive. It basically gives the identity of the compound present in the sample and also the shape and

size of the particle. The photoelectrodes prepared on ITO glass substrates from Approaches I, II and III were cut to a size that fits in the XRD cup and then mounted firmly in the cup with wax. XRF analysis of our sample showed 97% of Titanium and XRD analysis showed that the titanium present is in the form of anatase phase TiO_2 . The results are given in the Figures 5.17, 5.18, and 5.19.

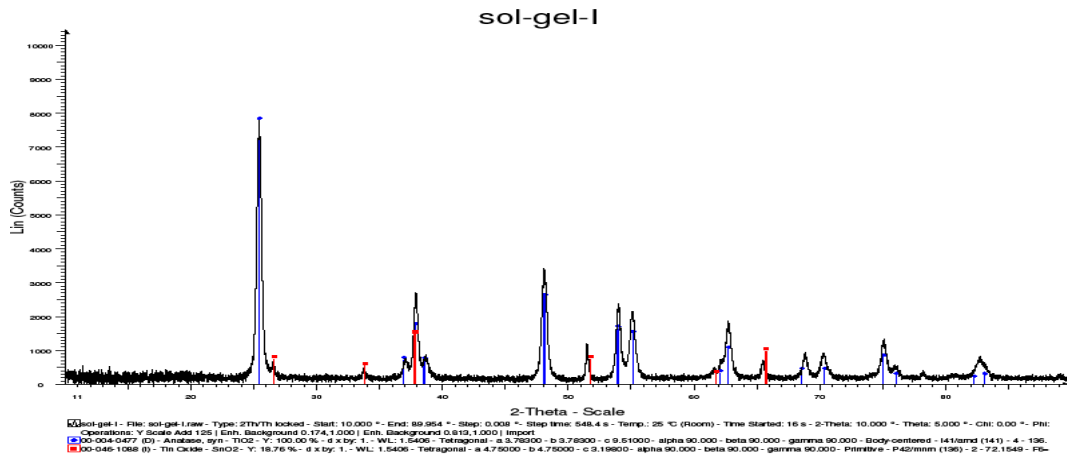


Figure 5.17: XRD pattern of TiO_2 sol-gel sample prepared from Approach I; blue lines correspond to anatase phase TiO_2 , while red lines correspond to SnO_2 .

Unit cell parameters of TiO_2 according to cif file:

Table 5.3: Unit cell parameters of TiO_2

Cell length "a"	3.78300
Cell length "b"	3.78300
Cell length "c"	9.51000
Crystal lattice	Tetragonal

Cell angle alpha, beta, gamma	90.000, 90.000, 90.000
-------------------------------	------------------------

Symmetry space group name	“I 41/amd”
---------------------------	------------

Symmetry Int tables number	136
----------------------------	-----

The XRD pattern in Figure 5.17 above was matched and refined to the pattern of anatase phase TiO₂ and SnO₂. The blue lines correspond to anatase phase TiO₂, while red lines correspond to SnO₂. Our TiO₂ sol-gel was coated on ITO conductive glass (indium doped tin oxide conductive glass substrates), thus the red lines in the XRD pattern correspond to ITO glass substrates.

5.7 Particle size calculation by using Scherrer formula:

Size of TiO₂ grain is important in developing a photoelectrode. Lower grain size gives maximum surface area. This can be studied using XRD analysis. After assigning the XRD pattern for the sample, the width of the peak was measured manually and substituted into the Scherrer equation [31]:

$$\tau = K\lambda/(\beta \cos \theta),$$

Where,

“ τ ” is particle size

“K” is the shape factor, X-ray diffraction patterns use shape factor in order to correlate the size of sub-micrometer particles in a solid to the broadening of a peak in a diffraction pattern.

“ β ” is the line broadening at half the maximum intensity (FWHM) in radians.

“ θ ” is Bragg angle.

The width of the peak is measured as 3 σ and the particle size is calculated as 23.8 ηm .

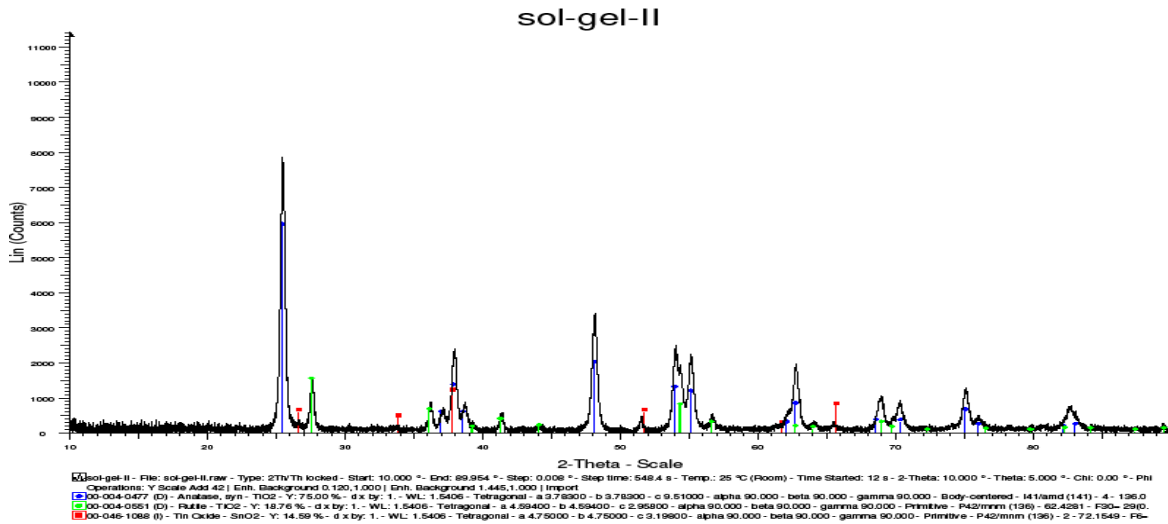


Figure 5.18: XRD pattern of TiO_2 sol-gel sample prepared from Approach II, blue lines correspond to anatase phase TiO_2 , green lines correspond to rutile phase TiO_2 red lines correspond to SnO_2 .

The XRD pattern in the Figure 5.18 above was matched and refined to the pattern of anatase and rutile phases of TiO_2 and SnO_2 . The blue lines correspond to anatase phase TiO_2 , Approach II utilized Degussa P-25 TiO_2 starting material, which contains both anatase, and rutile phases thus the green lines correspond to rutile phase TiO_2 and the red lines correspond to SnO_2 . Our TiO_2 sol-gel was coated on ITO conductive glass (indium doped tin oxide conductive glass substrates), thus the red lines in XRD pattern correspond to ITO glass substrates.

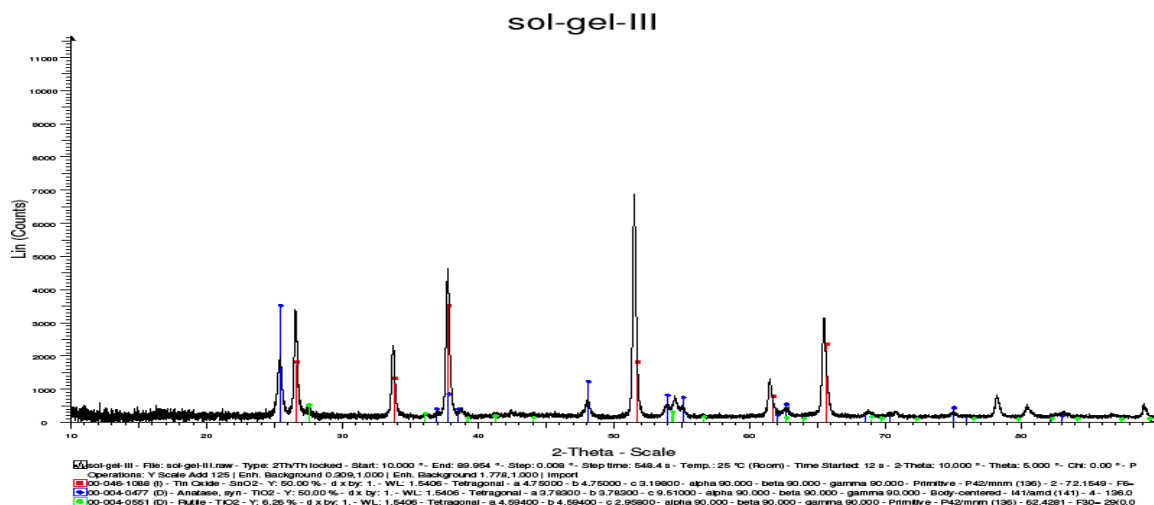


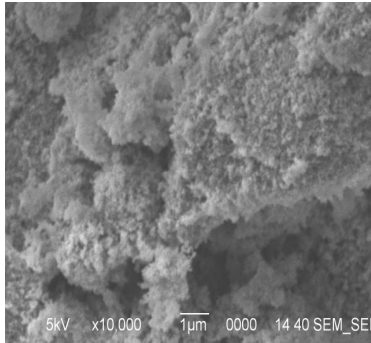
Figure 5.19: XRD pattern of TiO₂ sol-gel prepared from Approach III, blue lines correspond to anatase phase TiO₂, green lines correspond to rutile phase TiO₂ red lines correspond to SnO₂.

The XRD pattern in the Figure 5.19 above was matched and refined to the pattern of anatase and rutile phases of TiO₂ and SnO₂. The blue lines correspond to anatase phase TiO₂, Even though approach III includes TTIP as starting material, we can still see rutile phases this might be due to a slow hydrolysis step caused by DEA or by incipient conversion of anatase to rutile at 400 °C, which suppresses the precipitation of oxides from the alcoholic titanium isopropoxide solution. The green lines correspond to rutile phase TiO₂ and the red lines correspond to SnO₂. Our TiO₂ sol-gel was coated on ITO conductive glass (indium doped tin oxide conductive glass substrates), thus the red lines in the XRD pattern correspond to ITO glass substrates.

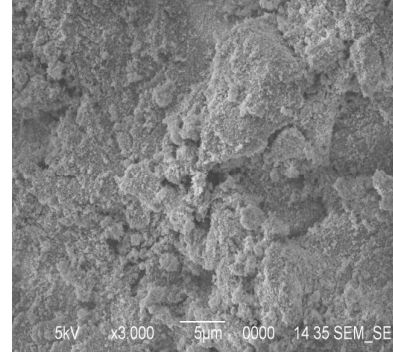
5.8 Morphology of TiO₂ films at microscopic level:

Scanning electron microscopic analysis was performed on our samples to compare the morphologies of the low temperature sol-gel to the conventional process. After sintering the films a 1'' x 1'' ITO glass substrate with TiO₂ film on it was cut and adjusted on to

the SEM sample holder. A copper tape was used in adjusting the sample substrate and also for conducting purpose.



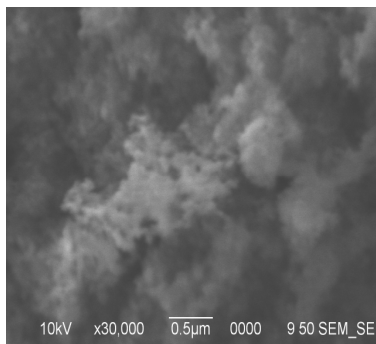
(A)



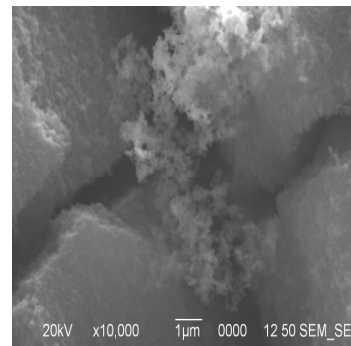
(B)

Figure 5.20: Images of TiO₂ sol-gel films prepared from Approach I, which are coated on ITO glass substrates.

The SEM micrograph in Figure 5.20 (A) shows a high magnification picture of TiO₂ sol-gel prepared from Approach I and sintered at low temperature, i.e., 150 °C, it mainly shows that the TiO₂ nanoparticles in a binder-free paste are well dispersed. Moreover the low magnification SEM image in Figure 5.20 (B) shows that these nanoparticles are well interconnected.



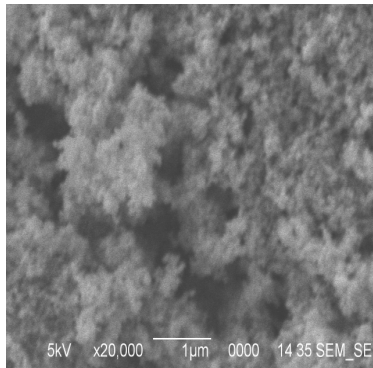
(A)



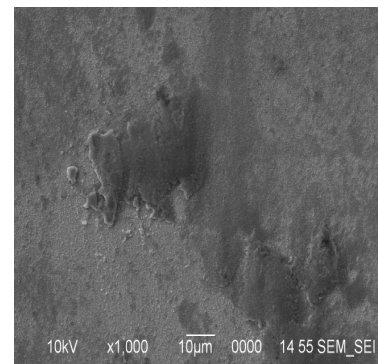
(B)

Figure 5.21: Images of TiO₂ sol-gel films prepared from Approach II, which are coated on ITO glass substrates.

The SEM micrograph in the Figure 5.21 (A) shows a high magnification picture of TiO₂ sol-gel prepared from Approach II and sintered at low temperature i.e. 150 °C. Figure 5.8.2 (A) is mostly identical to TiO₂ sol-gel prepared from Approach I, which confirms the same results in both approaches. Moreover the low magnification SEM micrograph which is shown in the Figure 5.21 (B) shows the same particle agglomeration phenomenon which can be seen in the sol-gel Approach I.



(A)



(B)

Figure 5.22: Images of TiO₂ sol-gel films prepared from approach III, which are coated on ITO glass substrates.

Thus when comparing the morphologies of films prepared from Approaches I and II with the morphology of films prepared from Approach III that is shown in the Figure 5.22 (A) and (B), the visual difference is hardly distinguishable. This tells us that the films prepared by low temperature processing of TiO₂ films gives the almost same result as of the film prepared by high thermal sintering process. Thus upon sintering at 150 °C, the acetate ions bridge the gap between the TiO₂ nanoparticles and in that process of sintering most of these ions are evaporated as ammonium acetate form just leaving a pure TiO₂ film on the substrate.

5.9 Photovoltaic measurements:

Photovoltage is measured by assembling the TiO_2 photoanodes in the cell, which is shown in Figure 5.23 below. The cell is connected to a potentiostat and placed under the solar simulator, which illuminates. The photovoltaic response/activity can be seen by the following voltammograms in Figures 5.9.2, 5.9.3 and 5.9.4. Also by using a multimeter (FLUKE 73 series II multimeter) we measured the photovoltage which is generated by the cell.

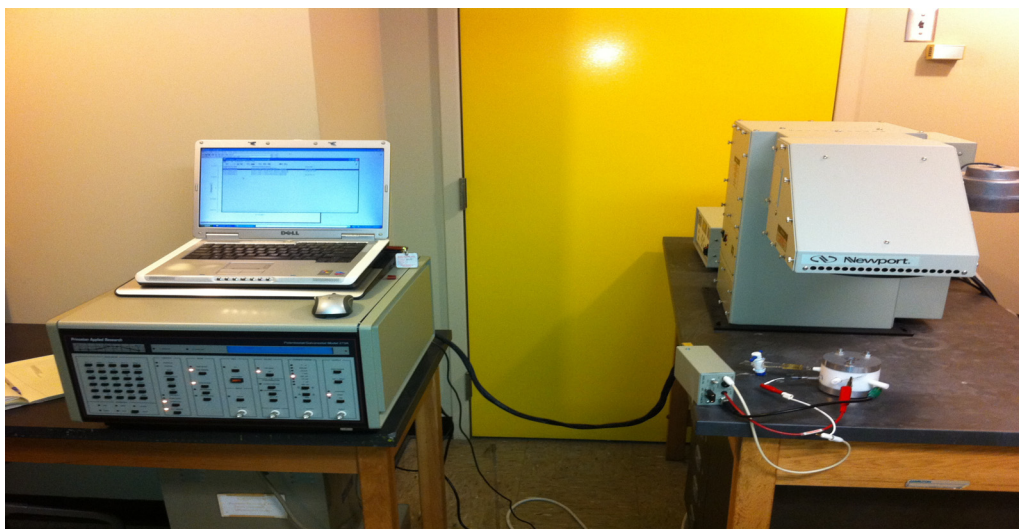
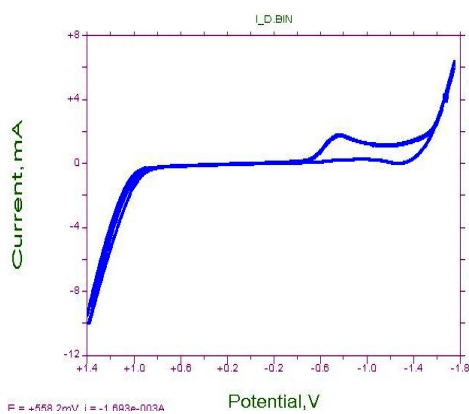


Figure 5.23: Photovoltaic measurements of TiO_2 photoanodes made by connecting and placing the cell with potentiostat and solar simulator.

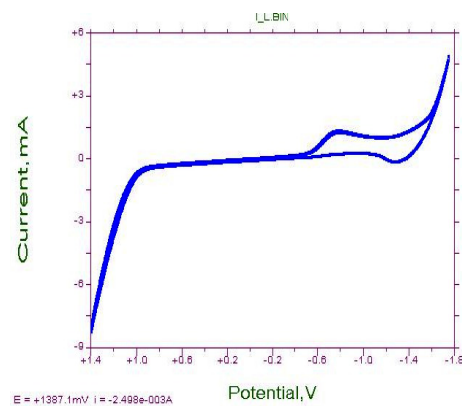
The voltammograms in the Figures 5.24, 5.25 and 5.26 shows reduction and oxidation activity of water in both dark and light environments. The electrolyte, sweep rate, reference electrode, counter electrode, working electrode and area of working electrode are tabulated in the following Table 5.4

Table 5.4: Details of photoelectrochemical cell.

Electrolyte	0.1 N NaOH
Sweep rate	50 mv/s
Reference electrode	Ag/AgCl electrode
Counter electrode	Platinum wire
Working electrode	TiO ₂
Area of working electrode	1.32 cm ²

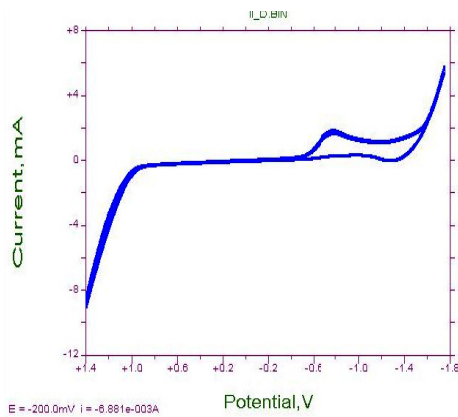


(A) Dark

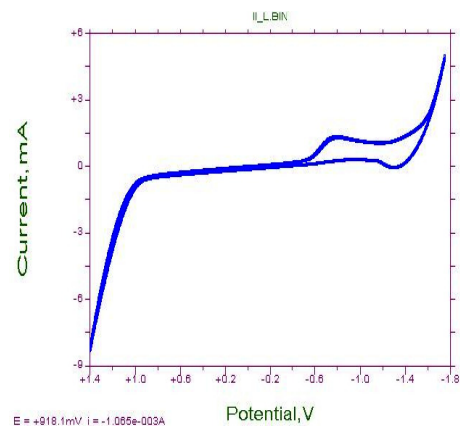


(B) Light

Figure 5.24: Voltammograms of TiO₂ photoanode in dark and light conditions prepared from sol-gel Approach I



(A) Dark



(B) Light

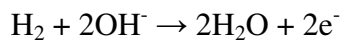
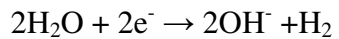
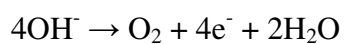
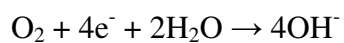
Figure 5.25: Voltammograms of TiO₂ photoanode in dark and light conditions prepared from sol-gel Approach II

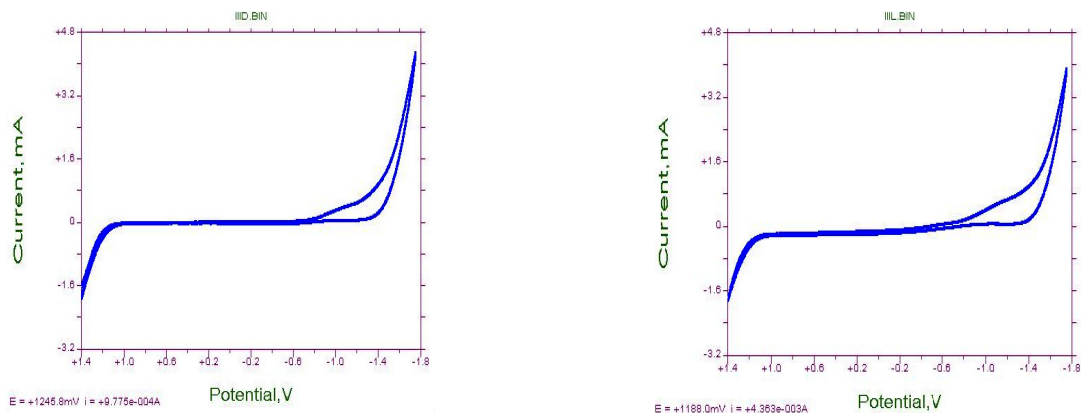
The voltammograms in Figures 5.24 and 5.25 shows that TiO₂ photoanodes prepared from sol-gel Approaches I and II has water reduction at peak -742.8 mV and oxidation took place at -1332.7 mV. Even though the Approaches I and II are different, the voltammograms in Figures 5.24 and 5.25 show the same reduction and oxidation activity for water in both dark and light conditions. However when we measured the photovoltage by using multi meter, we observed different photo voltages. The photovoltages are measured by connecting the positive and negative terminals of multimeter with platinum counter electrode and TiO₂ photoanodes of the cell. The voltages measured were summarized in the following table 5.5

Table 5.5: Photo voltages of TiO₂ photoelectrodes prepared from Approaches I, II and III

Approach	Dark	Light
TiO₂ photoanode prepared from sol-gel Approach I	20 mV	329 mV
TiO₂ photoanode prepared from sol-gel Approach II	29 mV	298 mV
TiO₂ photoanode prepared from sol-gel Approach III	59mV	583mV

Overall reactions are summarized below:





(A) Dark

(B) Light

Figure 5.26: Voltammograms of TiO₂ photoanode in dark and light conditions prepared from sol-gel Approach III

The sol-gel approach III is our conventional high temperature sintering approach, Figures 5.26 (A) and (B) shows reduction and oxidation activity for water in both dark and light conditions. The photovoltages measured in dark and light conditions by the multimeter are tabulated in table 5.5. Thus by comparison the TiO₂ photo anodes prepared from Approaches I and II has similar performance with Approach III.

Chapter 6

6.1 Conclusion:

The TiO₂ films prepared from the sol-gel Approaches I and II are strongly adhered to ITO substrates just similar to Approach III. This is evident by comparing the microscopic morphologies of films prepared from Approaches I and II with the film prepared from Approach III. Also the films survived the Scotch tape test, which confirms that the film is reasonably adhered to ITO substrate. The TiO₂ film prepared from Approach II has 17.86 % of rutile phase which lower the photovoltaic performance, but the film prepared from Approach I has 97% anatase phase, which is a successful acceptance for photovoltaic

measurement. On the whole we substantiated a low temperature sintering approach for developing TiO₂ films which are used in water splitting photoelectrochemical cells, DSSC's and for other purposes.

6.2 Future aspects:

The films prepared from Approach I and II has achieved photo voltage of 329 mV and 298 mV with pure TiO₂ films however this can be increased by dye sensitization of these films. Also developing a new configuration, where the electrode materials are interspersed as fused microelectrodes within a free-standing solid perforated polymer membrane like Nafion. This cell configuration avoids the use of external wiring to make contact between paired electrodes, yet preserves the intrinsic separation of products that electrochemistry affords. Conversion of rutile phase to anatase phase in Approach II, selection of appropriate dye, sensitization of the titania semiconductor and flexible configuration of cell would be the possible future aspects.

Chapter 7

7. References:

- 1) J, O. (2005). Hydrogen energy cycle : An overview . *Journal of Material Resources* , **20(12)**, 3167-3179.
- 2) Zhonghai Zhang, M. H. (2010). Photoelectrochemical water splitting on highly smooth and ordered TiO₂ nanotube arrays for hydrogen generation. *International journal of hydrogen energy*, **35**, 8528-8535.
- 3) J. Nowotny, T. M. (2007). Titanium dioxide for solar-hydrogen I Functional properties. *International Journal of Hydrogen Energy*, **32**, 2609-2629.
- 4) Slattery, D. K. (1999). *Photocatalytic Decomposition of water using organic pigments* . Florida: University of Central Florida.
- 5) K.Honda, A. (1972). TiO₂ Photochemistry and Photocatalysis. *Nature*, **238**, 37-39.
- 6) B.O'Regan, M. (1991). A Low -cost, high-efficiency solar cell based on dye sensitized colloidal TiO₂ films. *Nature*, **353**, 737-739.
- 7) Gratzel., K. K. (1998). Transition metal complexes from solid state synthesis. *Coordination Chemistry Reviews*, **77**, 347-414.
- 8) S. Nakade, W. K. (1993). Nanostructured materials for solar energy conversion. *Journal of American Chemical Society*, **107**, 6382.
- 9) Gratzel, M. (2005). Solar Energy Conversion by Dye-Sensitized Photovoltaic Cells. *Inorganic Chemistry*, **44(20)** 6841-6851 .
- 10) M.K. Nazeeruddin, A. K.-B. (1993). Chlorophyll-sensitized microporous cuprous iodide photocathode. *J. Am. Chem. Soc*, **115**, 6382.
- 11) Gratzel, M. (2009). Regeneration of Oxidized Organic Photo-Sensitizers in Grätzel Solar Cells: Quantum-Chemical Portrait of a General Mechanism. *Acc. Chem. Res*, **42** (11), 1788-1798 .
- 12) Ma., C. (2007, July Thursday). New Flexible Plastic Solar Panels Are Inexpensive And Easy To Make. *Science Direct* , pp. 42-45.
- 13) Mao, X. C. (2007). Titanium Dioxide Nanomaterials: Synthesis, properties modifications and applications. *Chem. Rev*, **107**, 2891-2959.

- 14) N.G. Park, J. v. (2000). Comparison of Dye-Sensitized Rutile- and Anatase-Based TiO₂ Solar Cells. *J. Phys. Chem.*, **104**, 8989-8994.
- 15) B. Seger, K. V. (2007). Fuel Cell Geared in Reverse: Photocatalytic Hydrogen Production Using a TiO₂/Nafion/Pt Membrane Assembly with No Applied Bias. *The Journal of Physical Chemistry*, **23**, (5471-5476).
- 16) Larminie, D. A. (2003). *Fuel cell Systems Explained*. West Sussex, England: John Wiley & Sons Ltd.
- 17) Krebs, F. C. (2009). Fabrication and processing of polymer solar cells : A review of print ligand. *Solar Energy Materials & Solar Cells*, **93**, 394–412.
- 18) Jeager, R. C. (2002). *Introduction to Microelectronics Fabrication - Modular Series on Solid-State Devices*.
- 19) Pavel Schilinsky, C. W. (2006). Performance Analysis of Printed Bulk Heterojunction Solar Cells . *Adv. Funct. Mater.*, **16**, 1669–1672.
- 20) Nam-gyu park, *. K.-J. (2005). Chemical Sintering of Nanoparticles: A methodology for low temperature Fabrication of Dye-Sensitized TiO₂ films . *Adv. Mater.*, **17**, 2349-2353.
- 21) E. Stathatos, P. C. (2004). Highly efficient nanocrystalline titania films made from organic/inorganic nanocomposite gels. *Microporous and Mesoporous Materials*, **75**, 255.
- 22) Arie Zaban, S. F. (1997). pH-Dependent Redox Potential Induced in a Sensitizing Dye by Adsorption onto TiO₂. *J. Phys. Chem.*, **101**(1), 55-57.
- 23) I. Bernacka-Wojcik, R. S. (2010). Inkjet printed and doctor blade TiO₂ photodetectors for DNA biosensors. *Biosensors and Bioelectronics*, **25**, 1229-1234.
- 24) I.M. Arabatzis, S. A. (2002). Photocatalytic Degradation of Organic Dye Methyl Orange with Phosphotungstic Acid. *Journal of Photochemistry and Photobiology*, **149**, 237-245.
- 25) A. I. Kontos, A. G. (2008). Nanostructured TiO₂ films for DSSCs prepared by combining doctor-blade and sol-gel techniques. *Journal of Materials Processing technology*, 196, 243-248.
- 26) P. Balraju, P. S. (2009). Effect of counter electrode, thickness and sintering temperature of TiO₂ electrode and TBP addition in electrolyte on photovoltaic performance of dye sensitized solar cell using pyronine G (PYR) dye. *Journal of Photochemistry and Photobiology*, **206**, 53-63.

- 27) Crouch, S. H. (2009). *Principles of instrumental Analysis*. Thomson.
- 28) A. Mabbot, G. (1983). *J. Chem. Educ. An Introduction to Cyclic Voltammetry.*, **60**, 697.
- 29) Vale´rie Gourinchas Courtecuisse, K. C.-F. (1996). Kinetics of the Titanium Isopropoxide Decomposition in Supercritical Isopropyl Alcohol. *Ind. Eng. Chem. Res.*, **35**, 2539-2545.
- 30) National institute of Standards and Technology (NIST) COBLENTZ NO: 4649
- 31) Patterson, A. (1939). "The Scherrer Formula for X-Ray Particle Size Determination". *Phys. Rev.*, **56(10)**, 978–982.